ALPHA FOUNDATION FOR THE IMPROVEMENT OF MINE SAFETY AND HEALTH

Final Technical Report

Project Title:	Proof-of-concept work to demonstrate optical microscopy with image analysis as a tool for semi-continuous coal mine dust monitoring
Grant Number:	AFC316FO-74
Organization:	Virginia Tech
Principal Investigator:	Emily Sarver
Co-principal Investigators:	Cigdem Keles (Virginia Tech) John R. Saylor (Clemson University)
Research Associate:	Nestor Santa (Virginia Tech)
Contact Information:	esarver@vt.edu, 540-231-8139
Period of Performance:	Oct 1, 2019 – Jan 31, 2021

1.0 Executive Summary

Motivation

Respirable dust exposure still represents a serious health risk to many mine workers. This fact has been highlighted by a dramatic resurgence of occupational lung disease among coal miners in central Appalachia, and has prompted calls for new dust monitoring technologies that can provide fast, preferably real-time, measurement of specific dust components, most notably crystalline silica.

To address the need for enhanced dust monitoring, we envision a novel device that combines established techniques in mineral identification and image analysis with capabilities in portable optical microscopy: in essence, a semi-continuous sampling device that collects dust particles on a substrate, periodically images them, and then processes the images to determine the relative abundance of coal and key mineral components, including silica. While the basic hardware required to build such a monitor could likely be adapted from existing devices, the ability to classify respirable coal mine dust particles by optical microscopy has heretofore not been investigated. This proof-of-concept project was thus aimed at demonstrating that optical light microscopy with image analysis can be used to count and classify the primary types of dust particles expected in a coal mine environment.

Research Approach

Based on previous dust characterization work sponsored by the Foundation, we considered that three primary sources are responsible for most of the respirable particles in underground coal mines: the coal strata, which contributes coal particles; the rock strata surrounding the coal, which contributes mostly silicates and silica; and the application of rock dust products to mine surfaces, which contributes mostly carbonates. To represent these sources, we used four high purity materials (i.e., coal, silica and kaolinite, and a real rock dust product) to generate respirable dust samples the microscopy work.

Following initial efforts to select an appropriate dust collection substrate and to standardize microscope lighting and imaging conditions, our work was keenly focused on establishing two classification models: one to distinguish coal from the mineral particles, and another to distinguish silica from the other minerals. We explored a wide range of candidate features for both models, and determined the most promising approach was to exploit relative differences in particle birefringence—an optical property associated with anisotropic materials, which causes them to illuminate under cross polarized light. All three of the minerals investigated here exhibit birefringence to some degree, however coal does not. Thus, by comparing images collected in plane and cross polarized light, it should be possible to distinguish coal from the minerals. Further, based on its relatively weaker birefringence, it should also be possible to distinguish silica from the other minerals.

Major Findings

We developed coal and silica classification models based on comparisons of greyscale particle intensities in plane and cross polarized image pairs collected under transmitted light. The coal model showed exceptional accuracy (overall 98%) when it was tested on images of known particles; and results were in very good agreement with those indicated by scanning electron microscope (SEM) for composite samples (i.e., containing coal and minerals). The silica model also showed good accuracy (overall 81%) when it was tested on images of known particles. Its performance was mixed on composite samples (containing coal plus minerals, or only minerals) compared to the SEM-derived results. We determined the reason for this outcome was relatively different particle densities in the images used for model development and those collected for the composite samples. We believe that effect of particle density can be quantified and accounted for in the silica model and/or dust sampling design, and plan to include this work in future research.

Impact

This project has demonstrated that optical microscopy could indeed serve as the basis for a novel monitoring concept. The envisioned monitor would allow quick identification of hazardous dust conditions, likely sources, appropriate interventions, and more efficient evaluation of dust controls.

2.0 Project Scope

This project is specifically related to the Foundation's focus on *Health and Safety Interventions*, and is informed by prior research[1] conducted under the *Injury and Diseases Exposure and Risk Factors* focus area.

2.1 Problem Statement

Respirable coal mine dust exposures have long been recognized as a major occupational health hazard. After decades of decline, a dramatic resurgence of lung disease among US miners began in the late 1990s (e.g., Attfield and Sexias, 1995; Antao et al., 2005; Suarthana et al., 2011). Prevalence and severity of disease has been particularly alarming in central Appalachian hotspots (e.g., Gamble et al., 2011; Blackley et al., 2014, 2016 and 2018). This geographic clustering combined with the radiographic evidence of disease has indicated that crystalline silica (i.e., quartz) exposures are a central factor in many cases (Pollock et al. 2011; Doney et al., 2019; Halldin et al., 2019). Several studies have suggested that silicates, which tend to co-occur with and are usually higher in abundance than silica, may also be important (e.g., Cohen et al., 2016; Jelic et al., 2017).

Near real-time measurements of total respirable dust concentration (mg/m^3) have recently become commonplace in coal mines thanks to the continuous personal dust monitor (CPDM). However, no such technology is available to monitor specific dust components. Compliance monitoring for quartz still requires laboratory analysis of filter samples, which means there is considerable lag time (i.e., days to weeks) between sample collection and results. In recognition of the need for faster results, NIOSH has developed a direct-on-filter (DOF) analysis method that uses a portable Fourier Transform Infrared (FTIR) instrument to measure quartz (μg) on filter sample at the end of a shift (e.g., Ashley et al., 2020; Cauda et al., 2016; Miller et al., 2017).

The CPDM and DOF quartz method represent major progress, but **monitoring capabilities are critically needed that provide even more timely information about specific dust components**. Such capabilities would allow quick identification of hazardous dust conditions, likely sources, appropriate interventions, and more efficient evaluation of dust controls.

2.2 Project Aim and Objectives

To address the need for enhanced dust monitoring, we envision a novel approach that combines established techniques in mineral identification and image analysis with increasing capabilities in portable optical microscopy: in essence, a semi-continuous sampling device that collects dust particles on a substrate, periodically images them, and then processes the images to determine the relative abundance of key components. While it is reasonable to assert the dust sampling and imaging hardware can be adapted from existing devices (e.g., air sampling pumps; mobile phone cameras as applied by, e.g., D'Ambrosio et al. 2015 or Switz et al., 2014), the ability to classify respirable coal mine dust particles by optical microscopy has heretofore not been investigated.

Thus, the specific aim of this project was to demonstrate that optical microscopy with image analysis can be used to count and classify the primary types of dust particles expected in a coal mine environment.

This work was inspired by common use of brightfield and polarized light microscopy for histologic analysis of tissue specimens. Of direct interest is successful use of such methods to distinguish between coal and mineral dust

[1] Research conducted on the following Foundation-sponsored projects has provided insights on respirable dust characteristics in underground coal mines: AFC113-11 (Connecting Dust Characteristics and Worker Health in Underground Coal Mining); AFC316-17 (Further Characterizing Respirable Coal Mine Particulates: Submicron Particles, Metals and Diesel Exhaust); AFC417-1 (Characteristics of Dust and Risk Factors Associated with the Development of Rapidly Progressive Pneumoconiosis and Progressive Massive Fibrosis).

particles (namely silica and silicates) in lung tissue specimens from miners with radiographic and/or pathologic evidence of occupational disease (e.g., Vallurupalli et al., 2013; Cohen et al., 2016; Jelic et al., 2017).

For the purposes of this work, we drew on comparisons previous research that generally indicates four main classes of respirable dust particles in coal mines, which can often be attributed to three major sources (Sarver et al., 2019) as shown in Figure 1. This paradigm serves as the basis for the particle classification scheme to be used in the envisioned dust monitor – and informed the specific research objectives on the current project. These included:

1. identify appropriate conditions for microscopy of coal and mineral dust particles;
2. establish and test classification model for distinguishing coal from any of the major types mineral dust particles expected in coal mine environments; and
3. establish and test classification model for distinguishing between the major types of mineral dust particles.

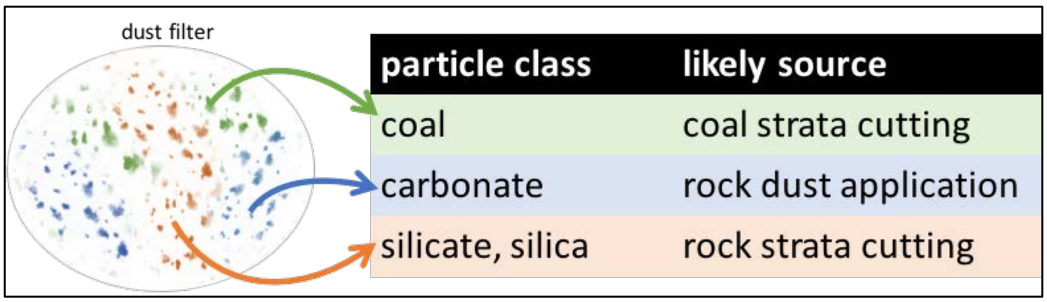

Figure 1. Conceptual illustration of scheme to classify dust particles into three major categories, each having a likely source.

3.0 Research Approach

Laboratory experiments were conducted in three phases to meet the project objectives. All optical microscopy was done with an Olympus BX53M Polarizing Microscope using its Stream Start (Version 2.3) software (Olympus, Center Valley, PA).

3.1 Initial Work to Identify Appropriate Microscopy Conditions (Objective 1)

3.1.1 Selection of substrate for dust sampling and imaging

The first task under this objective was to select a substrate for dust particle sampling and direct imaging. Four candidate materials were considered: glass, track-etched polycarbonate (PCTE), track-etched polyester (PETE) and polytetrafluoroethylene (PTFE, or "Teflon"). The glass was in the form of very thin coverslips; the other materials are filters made for air sampling.

Figures Figure 2-Figure 5 show images of an "orientation plate" sitting on each media, and under different lighting conditions (i.e., plane-polarized transmitted light, and cross-polarized transmitted light at 15° rotation intervals). The orientation plate serves as a standard surrogate for an anisotropic (birefringent) particle in these images. As it is rotated under polarized light, its brightness and color should change characteristically. The substrates themselves also have some characteristic behavior. The glass appears black at every rotation angle because it is amorphous and does not respond to polarized light. The PETE changes from bright purple to near black between 0 and 30°, indicating that it is birefringent. The PCTE and PTFE appear as shades of blue at every angle with nearly imperceptible changes. While calibration and correction for apparent color (and color changes) under polarized light might certainly be possible for any of the three filters, this added requirement (versus glass) may present significant challenges.

Moreover, it is noted that the images of the orientation plate on filter substrate in FiguresFigure 2-Figure 5 may be somewhat misleading in terms of expected results for respirable sized dust particles. These images were taken with the focus on the orientation plate, which is relatively thick. When the microscope was instead focused on the filter (top left of each figure), the features of each media become much more apparent (e.g., pores in the PCTE and PETE, and tracks in the PTFE) – and these may challenge the ability to identify and characterize very small dust particles. The glass generally does not have impurities or defects that should interfere with particle analysis.

Finally, while the glass serves as a rigid substrate, the filters are flexible. In order to prevent movement of the filters and keep them flat during imaging (to achieve good focus), we found it necessary to place a glass coverslip over them. This requirement might prove impractical for the envisioned semi-continuous monitor.

Considering all of the above, we selected glass as the optimum sample substrate for all further work. A glass substrate allows for imaging in reflected or transmitted light, with and without polarization, and it does not itself exhibit birefringence that might interfere with any dust particle analysis that attempts to exploit this property.

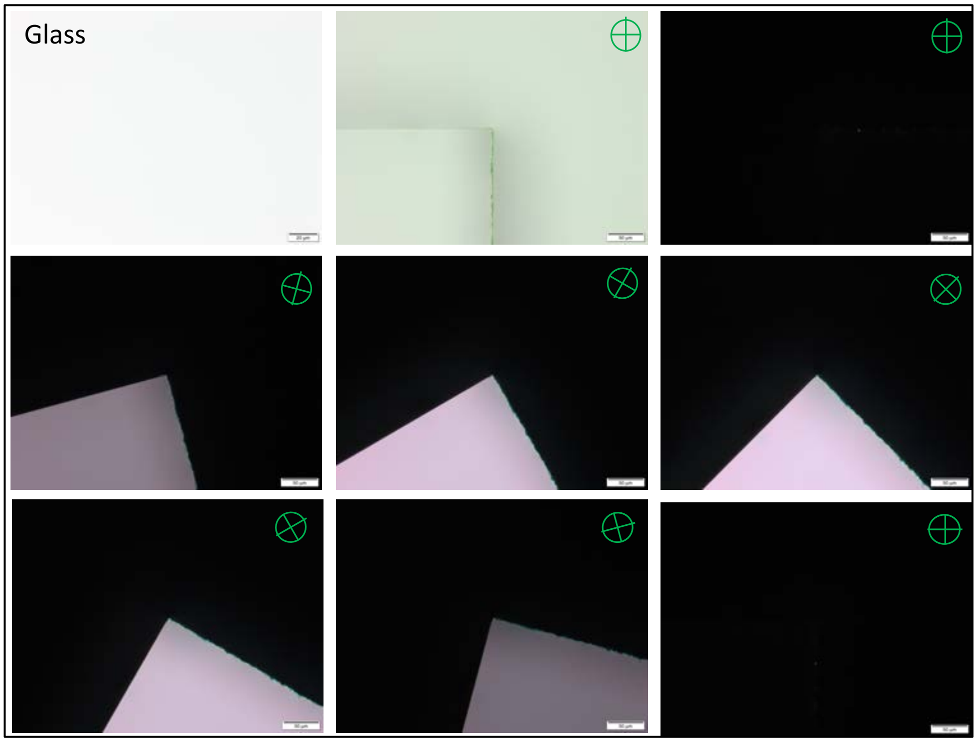

Figure 2. Top left: glass coverslip; Top center to bottom right: orientation plate on glass slip under transmitted non-polarized light at 0° rotation, then cross-polarized light at 0, 15, 30, 45, 60, 75 and 90° rotation.

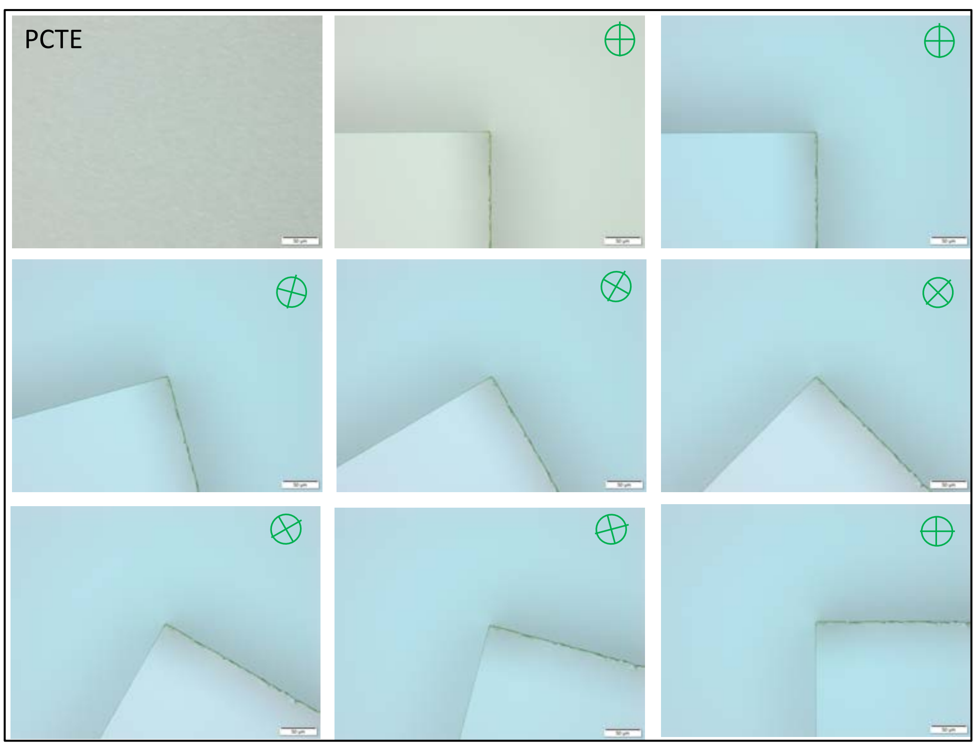

Figure 3. Top left: PCTE filter; Top center to bottom right: orientation plate on PCTE under transmitted non-polarized light at 0° rotation, then cross-polarized light at 0, 15, 30, 45, 60, 75 and 90° rotation.

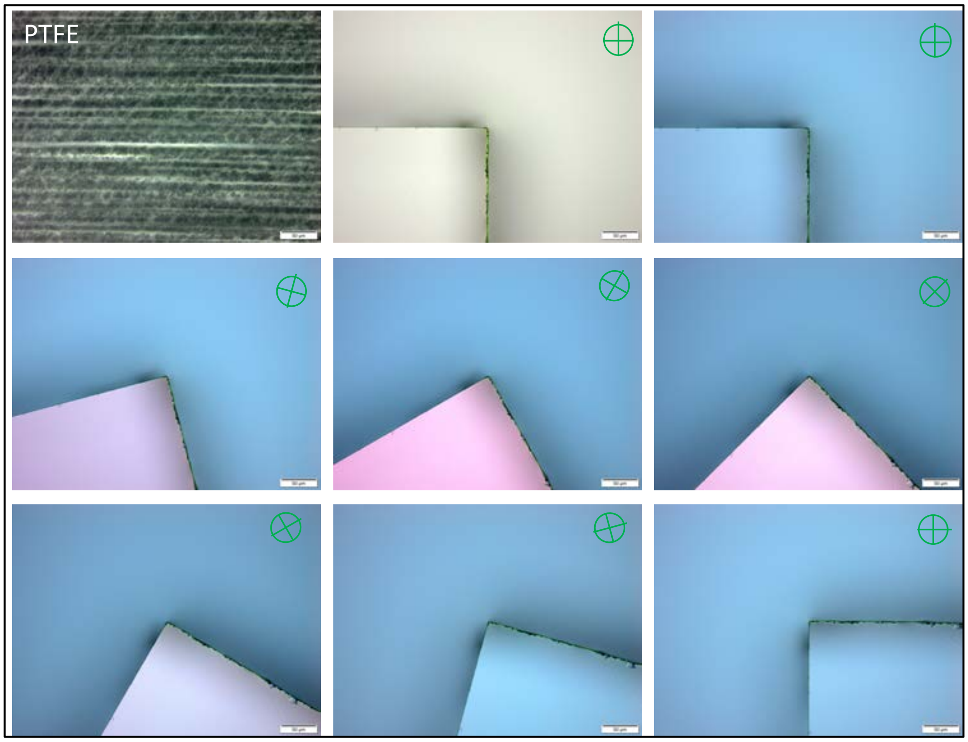

Figure 4. Top left: PTFE filter; Top center to bottom right: orientation plate on PTFE filter under transmitted non-polarized light at 0° rotation, then cross-polarized light at 0, 15, 30, 45, 60, 75 and 90° rotation.

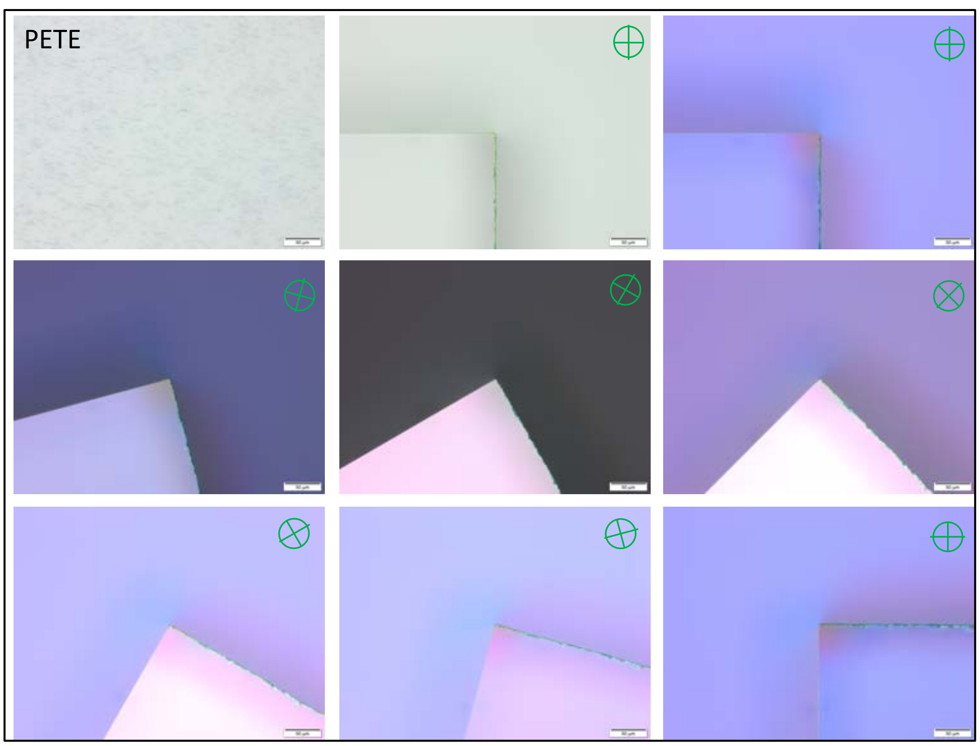

Figure 5. Top left: PETE filter; Top center to bottom right: orientation plate on PETE filter under transmitted non-polarized light at 0° rotation, then cross-polarized light at 0, 15, 30, 45, 60, 75 and 90° rotation.

3.1.2 Standard methodology for dust sampling and imaging

Following selection of the glass substrate, it was necessary to standardize a method for dust sampling onto the substrate – and also to standardize the imaging conditions and image handling.

Dust sampling. For dust sampling, we determined respirable-sized particles could be directly collected onto a small piece (i.e., ~5-12mm) of a glass coverslip (Figure 6). The glass piece was placed on top of a 37-mm PC filter in a standard 2-piece styrene cassette, which is used to sample from an enclosure at 2.0 LPM with a Dorr-Oliver cyclone. Following sample collection, the glass was carefully removed and mounted on top of a microscope slide for imaging under the optical microscope. The PC filter (which sampled the same dust) could also be used for analysis under the scanning electron microscope (SEM), as discussed later.

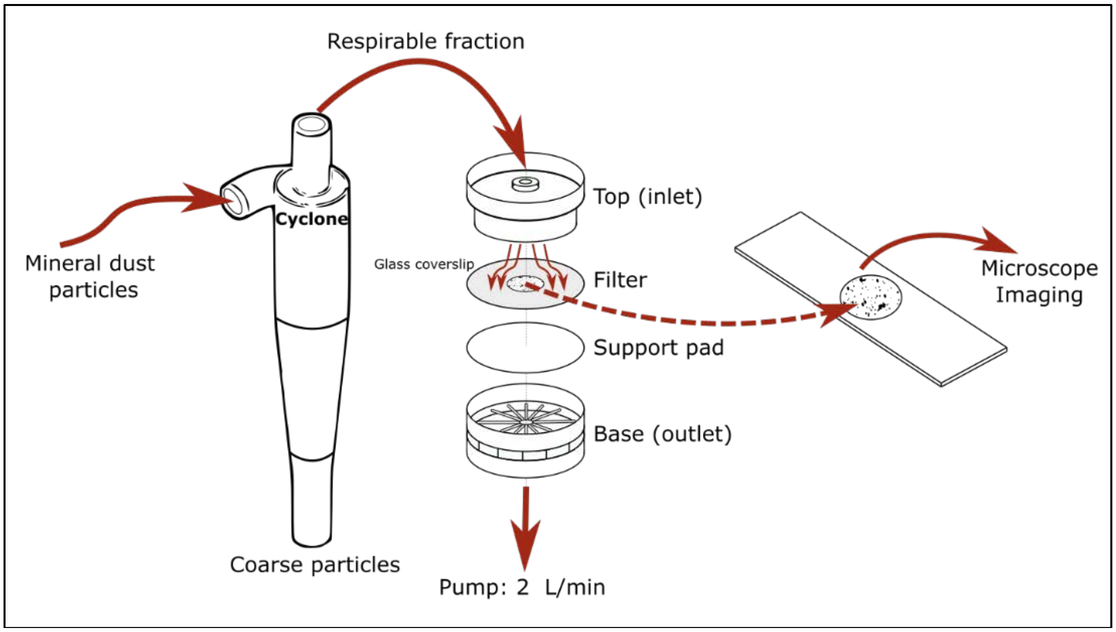

Figure 6. Dust sampling train.

Imaging. To ensure that reliable comparisons can be made between optical microscope images, standard settings for imaging and image handling were established as follows:

- **Basic microscope settings** – these are associated with lighting and magnification
  - Condenser aperture: 0.4
  - Objective magnification: 40X
  - Light intensity: 50%
- **Exposure time** – this affects the light intensity and contrast of images, and has been standardized for each combination of lighting mode and polarization to avoid saturation
  - Transmitted/unpolarized: 30.51 ms
  - Transmitted/polarized: 815.06 ms
  - Reflected/unpolarized: 12.99 ms
  - Reflected/polarized: 122.44 ms

- **Color balance** – this affects color contrast of images and was set obtaining an image of a clean coverslip on a blank glass slide, while illuminated by the camera's white LED light source set at 50% of its maximum intensity
    - Red channel: 1.81
    - Green Channel: 1
    - Blue Channel: 1.28
    - Saturation: 1
- **Image file type** – this affects image compression/preservation of data
    - TIFF file type (preserves all data)
    - 12-bit depth

It is noted that with the 40x objective and a 10x eyepiece, we achieved a total magnification of 400x. Each image had a resolution of 2560 x 1920 pixels, which corresponded to a spatial calibration of approximately 88 nm/pixel. Preliminary imaging of respirable dust particles indicated that particle identification (i.e., versus the glass background) was indeed feasible, and all further work proceeded using only respirable-sized dust.

3.2 Coal versus Mineral Classification (Objective 2)

Work under Objective 2 was aimed at simply distinguishing coal dust particles from particles of any of the primary mineral types expected in coal mine environments.

3.2.1 Dust source materials and sampling

Per Figure 1, we approached this proof-of-concept project from the perspective that just a few key sources are likely to generate most of the respirable dust particles in coal mines. However, the dust from each source differs in composition and may pose relatively different health hazards:

- The first and most obvious is coal seam itself, which generates predominantly coal particles upon cutting or breaking. Coal dust has long been considered a primary agent in the development of occupational lung disease (e.g., Petsonk et al., 2013; Beer et al., 2017).
- Rock strata that are often cut along with the coal seam or drilled during roof bolting can also contribute significant dust (Sarver et al., 2019; Johann-Essex et al., 2017a). These typically include shales, sandstones, and slates, which can yield dust dominated by silicates and/or silica. Depending on the particular geology, other minor constituents may also be present (e.g., heavy minerals, carbonates, etc.) Toxicity of crystalline silica is well established and linked specific forms of occupational lung disease in coal miners (e.g., Mischler et al., 2016; Beer et al., 2017). Moreover, recent evidence from studies of dust burden in the lungs of severely diseased miners suggests that silicates may also play a role in disease pathology (e.g., Cohen et al., 2016; Jelic et al., 2017).
- A third source of dust in coal mines is the application of rock dust products, which are typically composed of high purity carbonates (e.g., limestone and/or dolomite). While these particles can account for large proportions of respirable dust in some locations, a recent study suggests that they are less hazardous than other mineral components such as silica (Khaliullina et al., 2019).

Ideally, the envisioned semi-continuous dust monitor could estimate the number fraction of particles in four classes: coal, silica, silicate, and rock dust. With this in mind, we designed all experiments under Objectives 2 and 3 using dust particles representative of these classes (Table 1).

Table 1. Description of source materials used to generate respirable dust particles in four classes of interest.

Dust class	Source material description
coal	Clean bituminous coal (obtained directly from an industry partner), pulverized and sieved to -230 mesh; verified as high-purity carbonaceous particles by SEM
silica	Mixture of Min-U-Sil 5 and Min-U-Sil 10 pure silica products (US Silica, Katy, TX, USA)
silicate	Kaolinite powder product (Ward's Science, Rochester, NY, USA)
rock dust	Limestone rock dust product (obtained directly from an industry partner); verified as high-purity Ca-carbonate particles by SEM and XRD

The sampling scheme shown in Figure 6 was used to collect respirable particles from each of the four dust source materials. For each material, a total of three samples were collected simultaneously (i.e., using three separate sampling trains) from a small enclosure in which the material was aerosolized. The sampling time was around 5 seconds, which was long enough to enable significant particle collection on the glass without agglomeration and interference between particles. The glass coverslip was carefully removed from each sampling train and mounted on a microscope slide for imaging. The PC filter from one or two trains was also prepared for analysis by SEM (see below).

In addition to the samples of each material, three composite samples were also generated for work under this objective. Each of these contained a mixture of coal and one of the three minerals (i.e., coal + kaolinite, coal + rock dust, coal + silica). To collect these samples, three sampling trains were used to simultaneously collect coal dust particles. Then, each train was used to collect dust from a different mineral source material. Again, the glass coverslips were carefully removed and mounted for imaging under the optical microscope; and the PC filters from all three trains were prepared for SEM analysis.

3.2.2 Dust imaging

All imaging was performed using the Olympus BX53M Polarizing Microscope and standard conditions noted above. For the single-material samples, images were obtained on 50 "frames" of view per sample (Table 2); and for the composite samples, images were obtained on 20 frames per sample. As illustrated in Figure 7, a set of four images were obtained for each frame corresponding to four separate lighting conditions: transmitted plane-polarized (TPP), transmitted cross-polarized (TCP), reflected plane-polarized (RPP), and reflected cross-polarized (RCP). This resulted in a total of 600 images of particles generated from each of the dust materials, and 80 images of particles in composite samples.

Table 2. Dust samples generated and imaged for Objective 2. The total particles count includes all particles measuring 27 or more pixels in Feret diameter based on the particle identification method described below.

Dust samples		Frames imaged/sample	Total particles identified (≥ 27 pixels)
Single material	Coal x 3	50	24573
	Kaolinite x 3	50	20125
	Rock dust x 3	50	20512
	Silica x 3	50	8835
Composite	Coal + Kaolinite x 1	20	329
	Coal + Rock dust x 1	20	303
	Coal + Silica x 1	20	3167

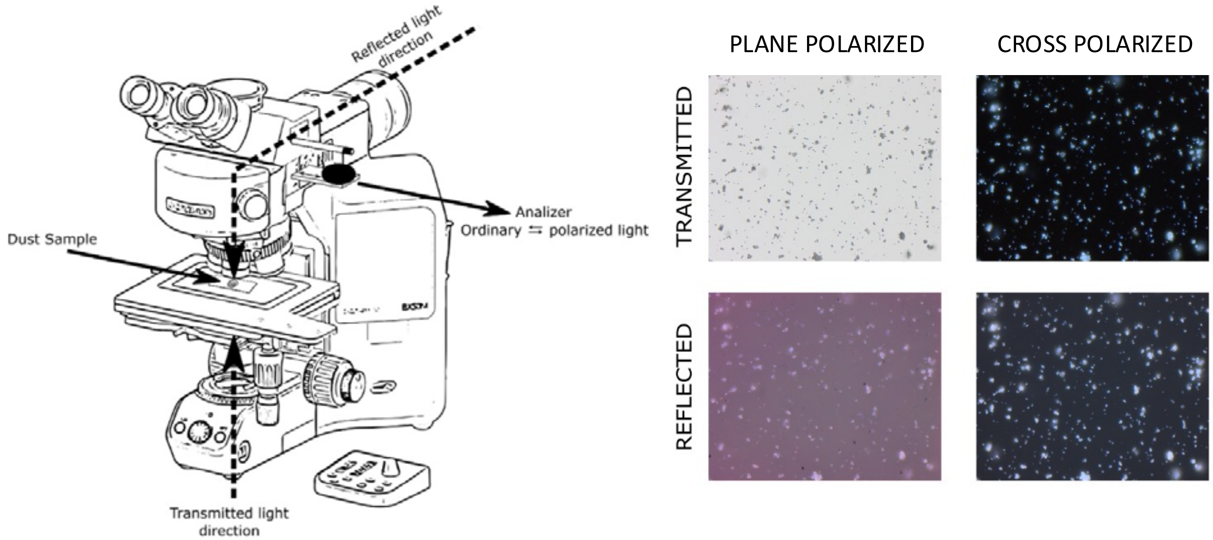

Figure 7. Microscope lighting conditions (left) and four image types obtained for each frame (right).

3.2.3 Image processing and classification model

To distinguish between coal and mineral particles, we exploited the phenomenon of birefringence. Under plane-polarized (PP) light, both coal and mineral particles can be distinguished from the background. However, under cross-polarized (CP) light, only anisotropic materials should illuminate. These include the main types of minerals components expected in respirable coal mine dust, but not the coal dust, which is amorphous. Thus, our approach under Objective 2 was to use the difference between PP-CP image pairs (i.e., in either transmitted or reflected light) to separate the coal and mineral dust. To do so, several steps were required: identify particles in each imaged frame, establish classification model(s) using the PP-CP image pairs obtained on single-material dust samples, and select the best pair for classification accuracy. All image processing was done using MATLAB®.

Identification of particles and extraction of characteristic features. For work under Objective 2, all images were first converted from RGB to greyscale. Then the greyscale intensities per pixel were input into an adaptive thresholding algorithm (available in MATLAB®) to identify particles (i.e., versus the background); this approach can account for any changes in the background intensities between images. The algorithm output is segmented image (i.e., binary mask) that effectively labels each pixel as particle or background. Binary morphological operations were performed to eliminate pixilation fuzz around particle boundaries and holes inside the particles. Holes were filled using pixel connectivity value of 4, and a dilation-erosion routine was applied iteratively for morphological closing.

Preliminary exploration showed that the TPP images had the best performance particle identification (i.e., as opposed to the TCP, RPP or RCP), so only TPP images were used for this task. Once the binary mask was created for each TPP image in a frame, it was applied to extract the grayscale intensities and locations for all particle pixels in all four images from the frame. Then the mean intensity for each particle (i.e., connected group of particle pixels) was computed and stored, as were a number of size and shape metrics. Based on preliminary analysis for particle classification efforts, a minimum particle size of 27 pixels (corresponding to a Feret diameter of about 2.38 µm) was used as a loose threshold for most subsequent work on the project – though the effect of particle size on classification accuracy was interrogated (see below). Using the 27-pixel size limit for particles, Table 2 shows the total number of particles identified in images of the samples containing only a single material, and in images of each composite sample.

It is also noted that a background correction was applied to the images in CP light, because we observed that the background intensity was often visibly brighter for images containing mineral particles. For this, we simply determined the mean greyscale intensity for all non-particle (background) pixels in an image, and then subtracted this value from *all* pixels.

Model development for coal versus mineral classification. As mentioned above, coal and birefringent mineral particles (including crystalline silica, most silicates, and the carbonates that dominate many rock dusting products) exhibit characteristic differences in particle illumination under PP and CP lighting conditions. As shown in Figure 8, the coal particles (left hand side of the images) appear relatively dark in the PP condition, and remain relatively dark in CP. On the other hand, mineral particles appear somewhat less dark in PP, and relatively bright in CP. Accordingly, we used a simple additive metric between the PP and CP particle intensities to establish a threshold between the coal and mineral particles: for each PP and CP image pair (transmitted or reflected light), the mean greyscale intensity for each particle was summed to determine the "aggregated mean particle intensity" or AMPI.

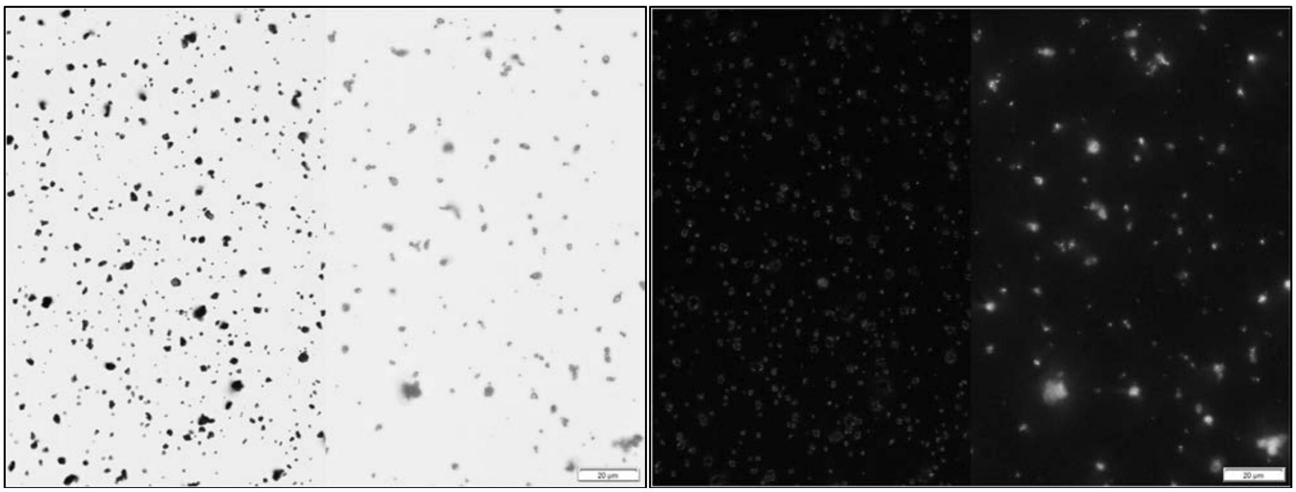

Figure 8. Example of dual images collected under (left) TPP lighting conditions and (right) TCP lighting conditions (background corrected). The left-hand side of each image contains only coal dust particles, and the right-hand side contains mineral particles.

To build a classification model based on the AMPI metric, the image dataset compiled from the single-material dust samples (150 frames for each material) was split into a training and test set (identically for both transmitted and reflected light conditions). The training datasets contained 90% of the image frames, within which a total of 63,848 particles (>27 pixels Feret diameter) were identified using the adaptive thresholding algorithm (see above); the remaining 10% of the frames (10,197 particles) were reserved to test the model performance.

Figure 9 shows the distribution of AMPI values for all coal and mineral particles used for model training. The optimal threshold was obtained by iteratively selecting AMPI values and computing the accuracy (defined as the number of correct classifications divided by the number of observations). The model using transmitted light PP and CP image pairs yielded an accuracy of more than 98% (within the training dataset), while the reflected light model only yielded about 88% accuracy. Thus, the transmitted light model was selected for further work under this objective.

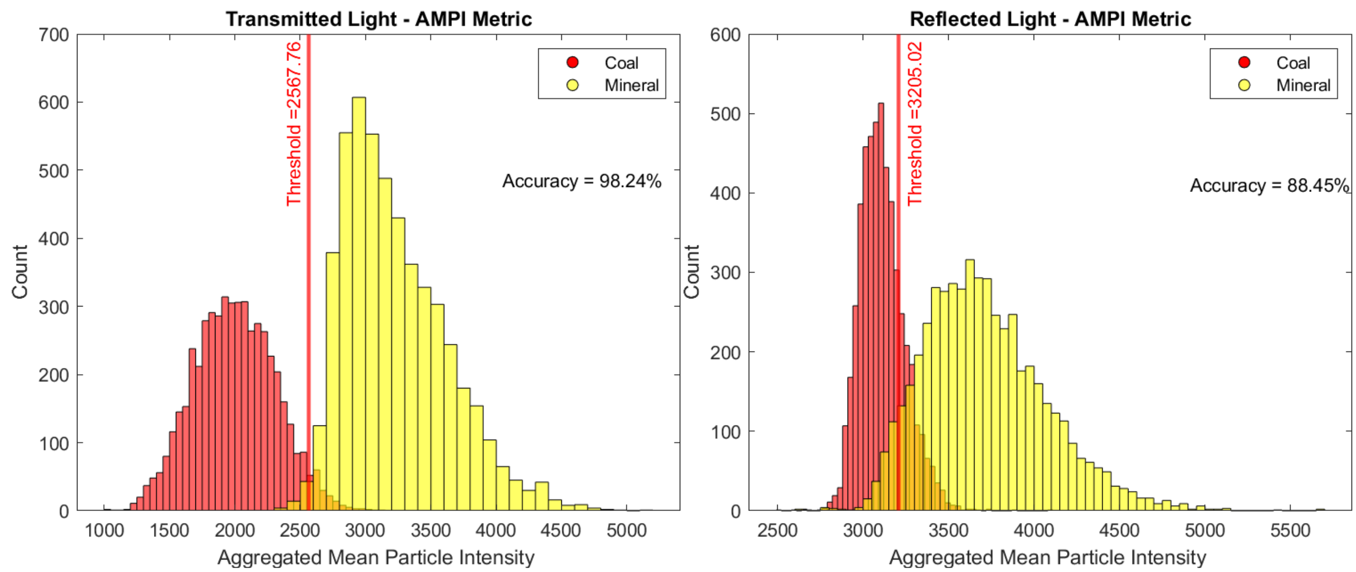

Figure 9. Distribution of AMPI for coal and mineral particles in the training datasets using transmitted (left) and reflected (light) PP and CP image pairs. The distribution includes the same 63,848 particles in both plots, with a lower size limit of 27 pixels. The overlapping area shows misclassification of particles.

From Figure 9, it is clear that coal particles are misclassified more often than mineral particles. Some of the brighter coal particles present AMPI values that intersect the lower limit of the AMPI distribution for mineral particles. This might be due to impurities in/on the coal dust particles that yield some illumination in the TCP images. Misclassification of mineral particles is less frequent but might be related to their relative orientation during imaging. If a mineral particle is oriented such that its vibration directions are closely aligned with the vibration directions of the polarizer and analyzer, this might result in light extinction – making the particle look dimer or darker under TCP lighting conditions.

The effect of particle size on the transmitted light classification model is shown in Figure 10. To include relatively smaller particles in the model, some accuracy must be sacrificed. Smaller particles are more difficult to classify since the optical resolution is limited to the objective magnification and image quality. However, the accuracy peaks at around 27 pixels (Feret diameter, which corresponds to about 2.38 µm). Based on these results, the 27-pixel size limit was kept for further testing of the model.

Finally, the transmitted light classification model was challenged using the test dataset (i.e., 10% of all frames reserved from the single-material dust sample images). Of the 10,197 total particles identified in this dataset, 4,951 (48.5%) were identified in the images of the coal samples and thus presumed to be coal; and the other 5,246 (51.45%) were identified in the images of the kaolinite, rock dust and silica samples and thus presumed to be mineral. The model misclassified 192 coal particles (4%) and 42 mineral particles (1%), yielding an overall accuracy of 98%. The high accuracy is visually illustrated in Figure 11.

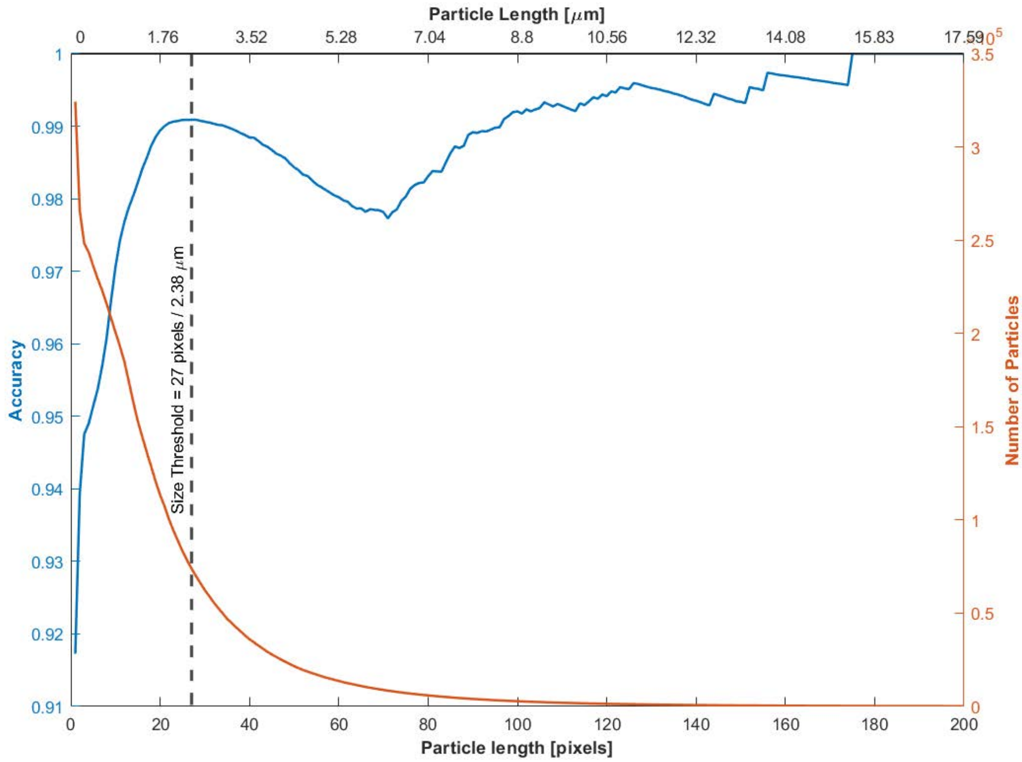

Figure 10. Effect of particle size on transmitted light classification model accuracy and number of particles included in the model.

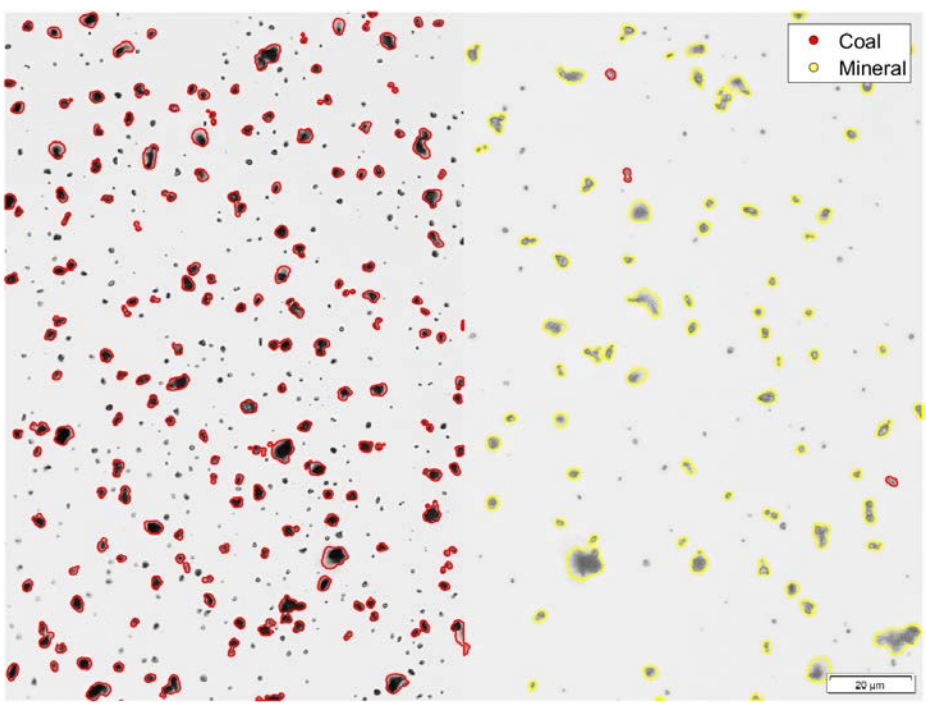

Figure 11. Example of the transmitted light AMPI classification model results on a dual image with only coal dust particles on the left and only mineral particles on the right. The classification results are superimposed on the same TPP images shown in Figure 8. Particles classified as coal are shown with red boundaries and those classified as mineral are shown with yellow boundaries.

3.2.3 Analysis by SEM-EDX

As explained above, when dust samples were generated on the glass coverslips for the optical microscopy work, samples were concurrently collected on PC filters for analysis by SEM with energy dispersive X-ray (EDX). One or two filters from each of the single-material samples, and all three composite sample filters were prepared and analyzed following the procedures detailed in Sarver et al., 2019.

Briefly, a 9-mm subsection of the sample filter was carefully cut, and sputter coated with Au/Pd. The samples were analyzed with a FEI Quanta 600 FEG environmental SEM (FEI, Hillsboro, OR) equipped with a Bruker Quantax 400 EDX spectroscope (Bruker, Ewing, NJ). A computer-controlled routine described by Johann-Essex et al. (2017b) was used to select, size, and classify about 500 particles (1-10µm) per sample using the classification criteria are shown in Table 3. The routine was run using Bruker's Esprit software (Version 1.9), and the following SEM settings: 1,000x magnification, 12.5 mm working distance, 15 kV accelerating voltage, 5.5 µm spot size.

Table 3. SEM-EDX particle classification criteria.

Particle Class		Atomic % by SEM-EDX							
		O	Al	Si	C	Mg	Ca	Ti	Fe
Carbonaceous	C	<29%	≤0.3%	≤0.3%	≥75%	≤0.5%	≤0.41%	≤0.06%	≤0.15%
Mixed carbonaceous	MC		<0.35%	<0.35%		≤0.5%	≤0.5%	≤0.6%	≤0.6%
Alumino-silicates	AS		≥0.35%	≥0.35%					
Silica	S*			≥0.33%					
Carbonate	CB	>9%				>0.5%	>0.5%		
Heavy minerals	HM		>1%					>1%	>1%

* Additional limits for S: Al/Si<1/3

Table 4 shows the SEM-EDX classification results on the single-material dust samples, which are displayed on a percentage area basis; this was calculated by summing the measured area of all particles in a given class and dividing by the total area of particles in all classes. Results for the single-material samples verify the high-purity of the materials used to generate the dust samples. As expected, coal particles were primarily classified as C and MC; kaolinite particles were classified as AS; rock dust was primarily classified as CB; and silica was classified as S. The composite sample results are also shown in the table and are compared later to the optical microscopy results in the research findings.

Table 4. SEM-EDX classification results on the single-material and composite samples containing coal plus one mineral.

Dust sample		Area % of all particles							Particles analyzed
		C	MC	AS	S	CB	HM	O	
Single material	Silica	0.3%	0.3%	0.0%	99.4%	0.0%	0.0%	0.0%	500
		0.1%	0.2%	0.0%	99.7%	0.0%	0.0%	0.0%	533
	Kaolinite	0.0%	0.0%	100.0%	0.0%	0.0%	0.0%	0.0%	550
	Rock dust	0.6%	1.0%	0.9%	0.0%	97.0%	0.0%	0.6%	500
		0.8%	0.5%	0.3%	0.0%	98.4%	0.0%	0.0%	550
	Coal	98.4%	1.4%	0.1%	0.0%	0.0%	0.0%	0.1%	550
		99.9%	0.1%	0.0%	0.0%	0.0%	0.0%	0.0%	550
Composite	Coal + Kaolinite	8.8%	17.4%	73.8%	0.0%	0.0%	0.0%	0.0%	500
	Coal + Rock dust	85.9%	1.4%	0.0%	0.0%	12.6%	0.0%	0.0%	500
	Coal + Silica	92.2%	2.6%	0.1%	4.8%	0.0%	0.0%	0.3%	500

3.3. Sub-Classification of Minerals (Objective 3)

Work under Objective 3 was aimed at distinguishing *between* the primary types of mineral expected in coal mine environments.

3.3.1 Dust source materials and sampling

The same single-material dust samples collected for work under Objective 2 (Table 2) were also used for work under Objective 3. In addition, composite samples were collected that contained all three mineral types of interest (i.e., kaolinite, rock dust and silica), as well as all three mineral types plus coal. The composite samples were collected using the same source materials (Table 1) and sampling procedures described above, sequentially collecting particles from each material. Again, samples for optical microscopy were collected on glass coverslips while concurrently collecting samples for SEM work on PC filters (Figure 6).

3.3.2 Dust imaging

For the single-material dust samples, the same optical microscope images collected for work under Objective 2 were used. For the new composite samples, the same microscope and standard settings outlined earlier were used for imaging. In each frame of view, images were again captured using the four lighting conditions shown in Figure 7 (i.e., TPP, TCP, RPP, RCP).

The total number of frames imaged for each of the single materials and for the composite samples is summarized in Table 5. For work under Objective 3, we investigated mineral classification using the same size threshold determined under Objective 2 (i.e., 27-pixel Feret diameter, about 2.38 µm). This limit yielded the total number of particles shown in Table 5.

Table 5. Dust sample images for Objective 3. (The single material samples and composite samples containing coal and one mineral are the same samples reported in Table 2.)

Sample Type	Material	Frames imaged/sample	Total particles identified (≥ 27 pixels)	Average particles per frame
Single material	Kaolinite x 3	50	24573	164
	Rock dust x 3	50	20125	134
	Silica x 3	50	20512	137
Composite (coal + one mineral)	Coal + Kaolinite x 1	20	329	16
	Coal + Rock dust x 1	20	303	15
	Coal + Silica x 1	20	3167	158
Composite (3 minerals)	K+RD+S (CS1)	20	5298	265
	K+RD+S (CS2)	20	6296	315
	K+RD+S (CS3)	20	5315	266
Composite (3 minerals + coal)	K+RD+S+C (CS4)	30	2702	90
	K+RD+S+C (CS5)	30	3432	114

3.3.3 Image processing and classification model

Identification of particles and extraction of characteristic features. The general process for particle identification and feature extraction is illustrated in Figure A1 in the Appendix. Briefly, the same adaptive threshold approach described above was used to identify and label particle pixels (again based on the TPP images). This time, the binary mask was used to extract particle pixel intensities in the red, green and blue (RGB) channels (in all four lighting conditions), in addition to just the greyscale intensity. With the RGB intensities, a series of color features was computed for each particle (in each lighting condition); and a number of particle size, shape and texture features were also computed. Moreover, MPI features (such as the AMPI described under Objective 2) were computed to compare the RGB and greyscale intensities of particles in the PP and CP image pairs. In total, some 41 features were considered for this work (Table A1).

Model development for mineral sub-classification. Initially, we explored the possibility of concurrently separating the three mineral classes (silica, rock dust and kaolinite). For this, an algorithm was coded in MATLAB® to analyze all the possible combinations of three features in the dataset that yields the best separation of mineral classes, given particular lighting conditions and particle size limits. To measure this separation, a figure of merit (f.o.m) was computed as the ratio of the mean linear distance between feature centroids and the root mean square (RMS) distance of each mineral cluster in 3D (Figure 12). The basic idea is that the combination of features with the highest f.o.m can be used to accurately separate the mineral classes.

Unfortunately, based on the features listed in Table A1, our f.o.m. values for 3-mineral models were generally quite low (<0.6), indicating relatively poor performance. However, simple correlation matrices did show promise for performing *binary separations*, especially for the case of separating silica particles from the other two minerals – which would certainly represent an exciting development for respirable coal mine dust monitoring. For example, the correlation matrices shown in Figure A2 illustrate clear differences between the transmitted and reflected light greyscale AMPIs. Thus, we decided to pursue silica classification with the intent of eventually constructing a two-step process: first separate coal from minerals, then separate silica from other minerals.

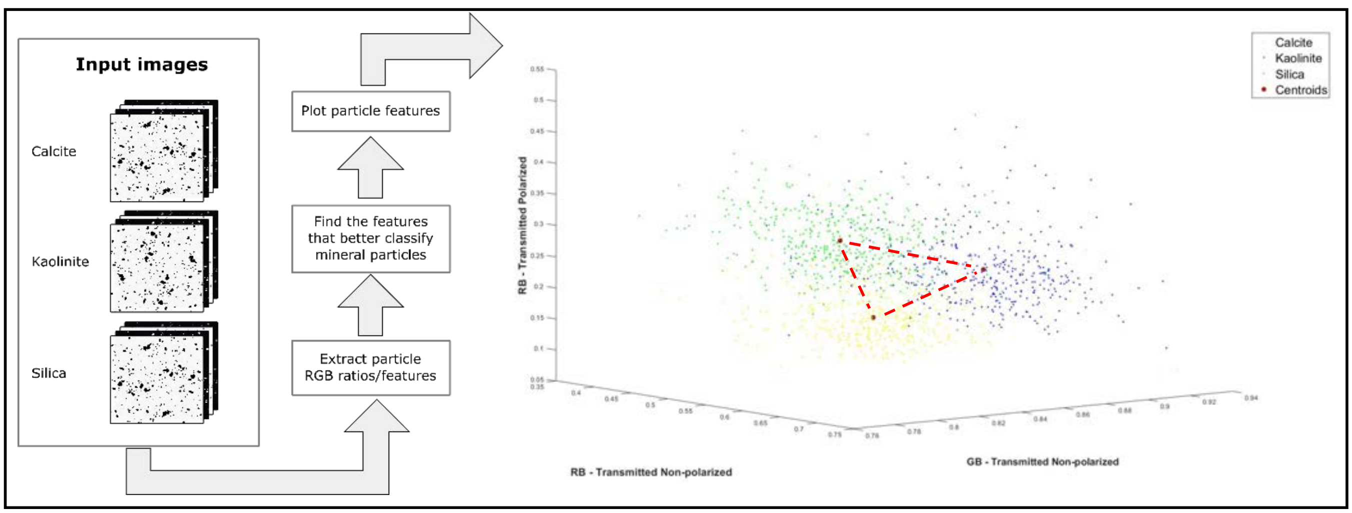

Figure 12. Hypothetical example of analysis and selection of classification features.

Table 6 shows the results of preliminary f.o.m. analysis on the possible binary separations for the minerals investigated on this project. The table includes the top-five features for separating all binary pairs, and the f.o.m. value is shown for each pair. The transmitted AMPI is the same feature used for the coal versus mineral separation under Objective 2. The transmitted MMPI is a similar feature, which multiplies the mean intensity of each particle in a TPP and TCP image pair; and the reflected DMPI represents the difference between mean intensity of each particle in a RPP and RCP pair. The TPP greyscale standard deviation (of pixels) and the homogeneity of any given particle were also identified as promising features.

Table 6. Top five features for binary separation of mineral classes. This analysis was conducted prior to any background correction of the CP images. (GSD = grayscale standard deviation.)

Feature	Kaolinite vs. Rock dust	Kaolinite vs. Silica	Rock dust vs. Silica	Kaolinite vs. other minerals	Rock dust vs. other minerals	Silica vs. other minerals	Mean f.o.m
Transmitted AMPI	0.382	1.24	0.805	0.538	0.096	0.981	0.67
Transmitted MMPI	0.285	1.22	0.946	0.453	0.015	1.056	0.66
TPP GSD	0.012	0.828	0.969	0.186	0.174	0.888	0.51
Homogeneity	0.583	0.537	0.065	0.568	0.437	0.273	0.41
Reflected DMPI	0.384	0.209	0.594	0.211	0.442	0.397	0.37

Based on Table 6, the transmitted light MMPI was chosen to separate silica from the other minerals (i.e., kaolinite and rock dust). Figure 13 shows TPP and TCP image pairs of silica and either rock dust or kaolinite particles. Compared to similar images shown in Figure 8, it is clear that the silica particles exhibit some birefringence compared to coal, but not nearly to the extent of the other two minerals.

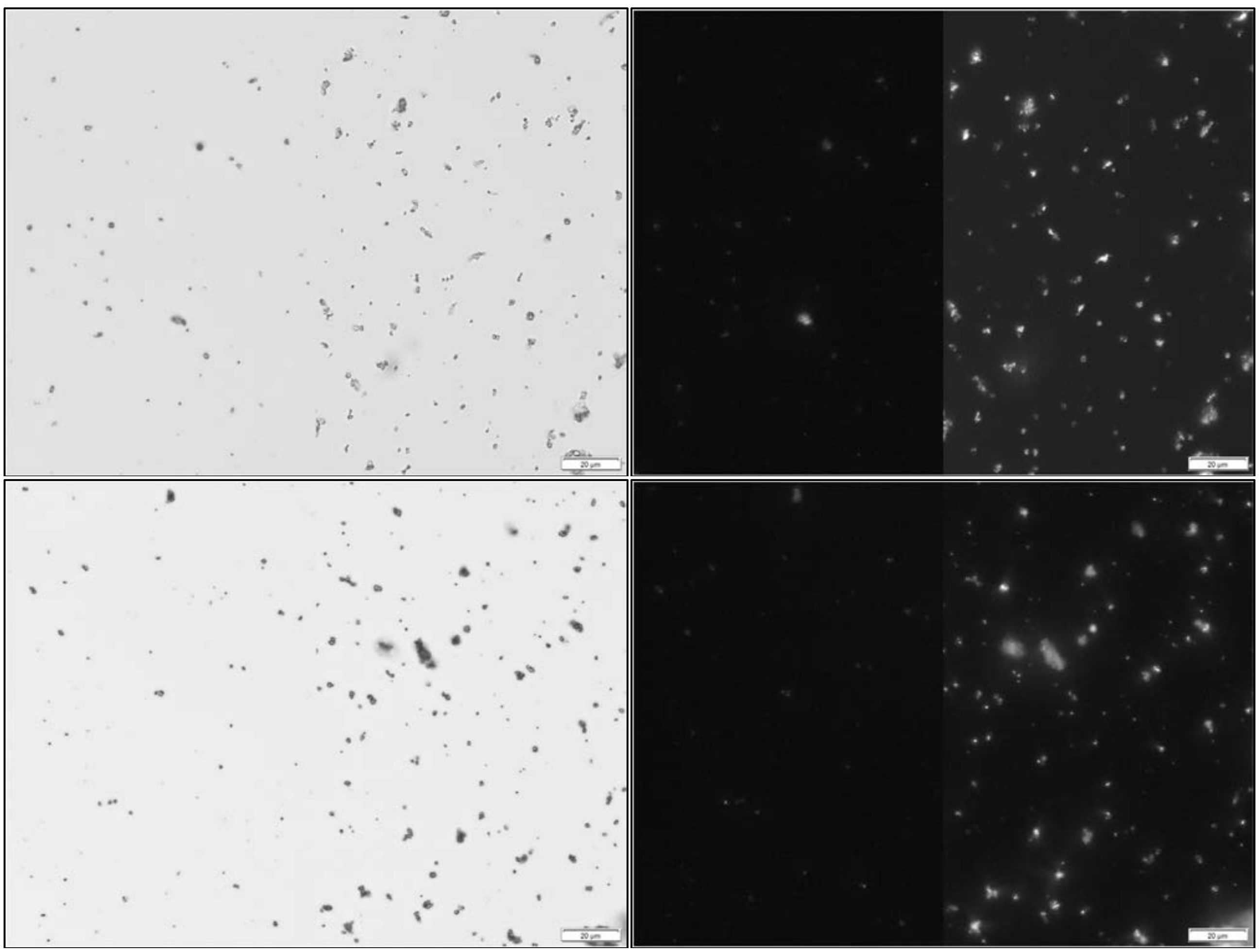

Figure 13. Two examples (top and bottom) of dual images collected under (left) TPP lighting conditions and (right) TCP lighting conditions (following background correction). The left-hand side of each image contains only silica dust particles, and the right-hand side contains either rock dust or kaolinite particles.

To build a silica classification model based on the MMPI metric, a similar approach was used for the AMPI model developed for coal versus mineral classification under Objective 2: The image dataset compiled from the single-material mineral dust samples (150 frames for each mineral) was split into a training and test set (identically for both transmitted and reflected light conditions). The training datasets contained 90% of the image frames, within which a total of 44,376 particles (> 27 pixels Feret diameter) were identified using the adaptive thresholding algorithm (see above); the remaining 10% of the frames (5,096 particles) were reserved to test the model performance.

The left side of Figure 14 shows the distribution of MMPI values under transmitted light for all mineral particles used for model training. The optimal threshold (0.85 E+06) was obtained by varying possible values and computing the accuracy for both the silica and other minerals; accuracy is defined as the number of particles classified into their correct class divided by the number of true particles in that class. At the optimum MMPI threshold, the model yielded an accuracy of 77% for both silica and the other minerals classes.

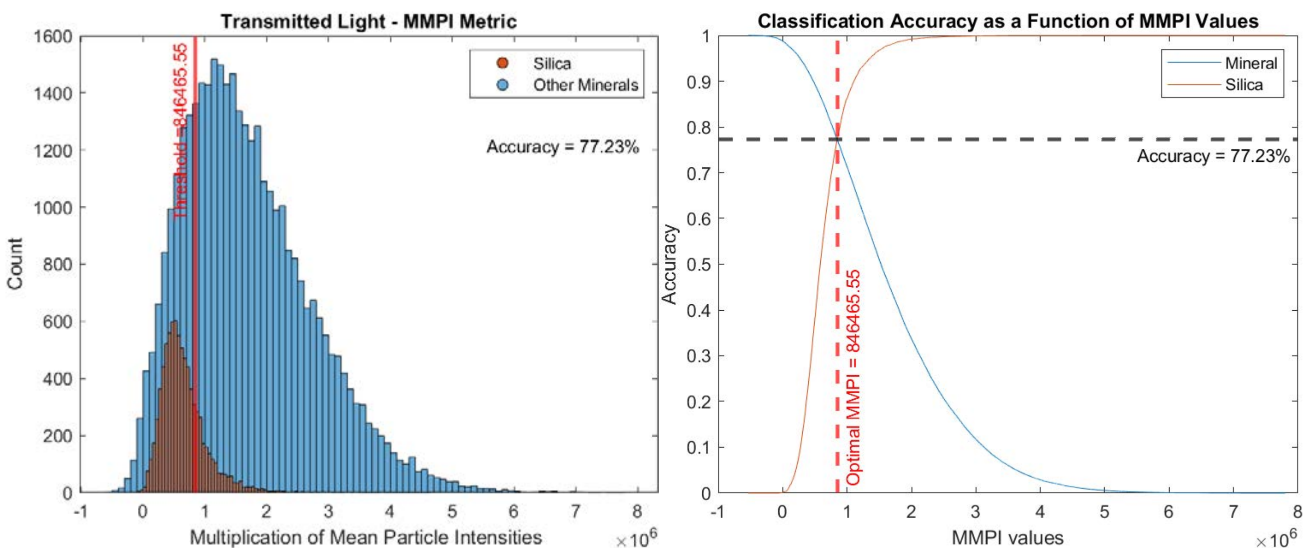

Figure 14. (Left) Distribution of MMPI metrics for silica and other minerals (kaolinite and rock dust) particles in the training dataset using transmitted PP and CP image pairs. The overlapping area shows misclassification of particles. (Right) Accuracy of silica and other minerals classification as a function of MMPI threshold selection.

When the model was run on the test dataset, the accuracy for silica classification was indeed 77% and accuracy for the other minerals slightly improved over what was predicted by the training dataset (Table 7). The overall accuracy was about 81%. Figure 15 shows examples of the MMPI classification model results on dual images of silica and either rock dust or kaolinite. The tendency for the current model to misclassify some silica particles as "other mineral" is clear. On the other hand, relatively few other mineral particles are misclassified as silica.

Table 7. Transmitted light MMPI silica classification model results on the training and test datasets using particles from single-material samples.

		Silica	Other minerals Kaolinite	Rock dust
Training set (77%)	True	8235	17831	18310
	Predicted	6361 (77%)	12875 (72%)	15038 (82%)
	Misclassified	1874 (23%)	4956 (28%)	3272 (18%)
Test set (81%)	True	600	2294	2202
	Predicted	463 (77%)	1808 (79%)	1868 (85%)
	Misclassified	137 (23%)	486 (21%)	334 (15%)

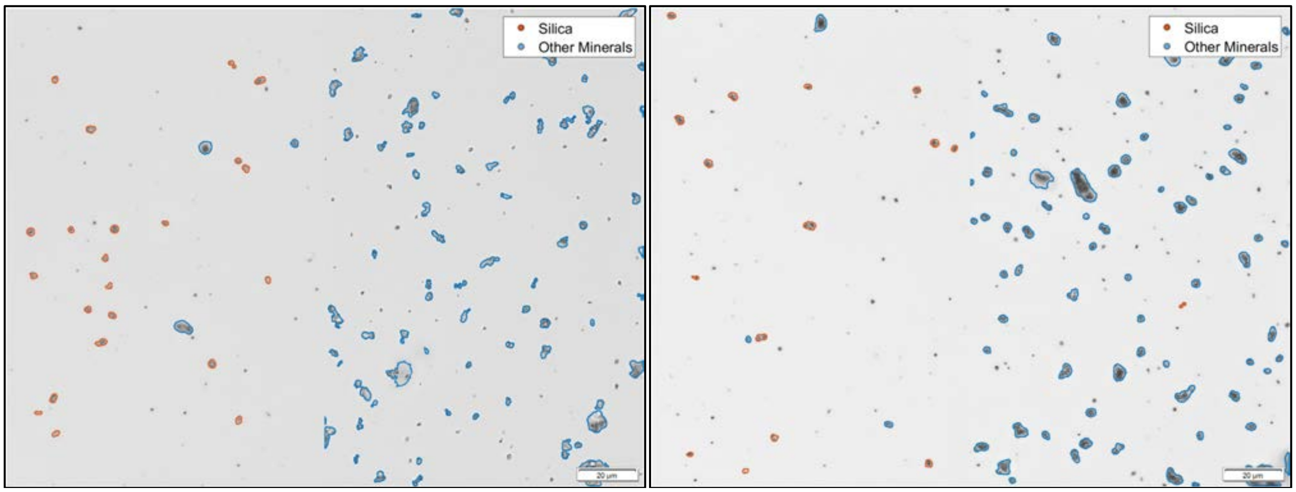

Figure 15. Examples of the transmitted light MMPI classification model results on dual images with only silica particles on the left-hand side of an image, and only kaolinite or rock dust particles on the right-hand side. The classification results are superimposed on the same TPP images shown in Figure 16. Particles classified as silica are shown with red boundaries and those classified as other mineral are shown with blue boundaries.

3.3.4 Analysis by SEM-EDX

The new composite samples containing all three minerals or all three minerals plus coal were analyzed by SEM-EDX using the same procedures described earlier and the criteria shown in Table 3. The results are given in Table 8.

Table 8. SEM-EDX classification results on the composite samples containing all three minerals or all three minerals plus coal.

Dust sample		Area % of all particles							Particles analyzed
		C	MC	AS	S	CB	HM	O	
Composite (3 minerals)	K+RD+S (CS1)	0	3	60	27	8	0	1	500
	K+RD+S (CS2)	0	1	74	21	4	0	2	500
	K+RD+S (CS3)	0	2	77	17	4	0	0	500
Composite (3 minerals + coal)	K+RD+S+C (CS4)	10	13	75	1	1	0	0	1000
	K+RD+S+C (CS5)	9	8	68	13	1	0	1	500

4.0 Research Findings and Accomplishments

Work under Objective 1 served as a fundamental basis for subsequent work and has been described in detail under Section 3.1. The major findings and accomplishments were:

- Glass is a suitable substrate for dust collection and imaging.
- It is possible to identify respirable-sized particles given the magnification power and resolution of the optical microscope used here.
- Standard settings for imaging on glass substrate and image handling were established.

4.1 Coal versus Mineral Classification (Objective 2)

The coal versus mineral classification model described in Section 3.2 was applied to the composite dust samples containing coal and one mineral (Table 2). Figure 17 shows and example of the results for one of the 60 image frames that were analyzed. Darker particles can be visually identified as coal particles, and brighter particles are believed to be mineral. The output of the algorithm visually matches with the expected particle identification.

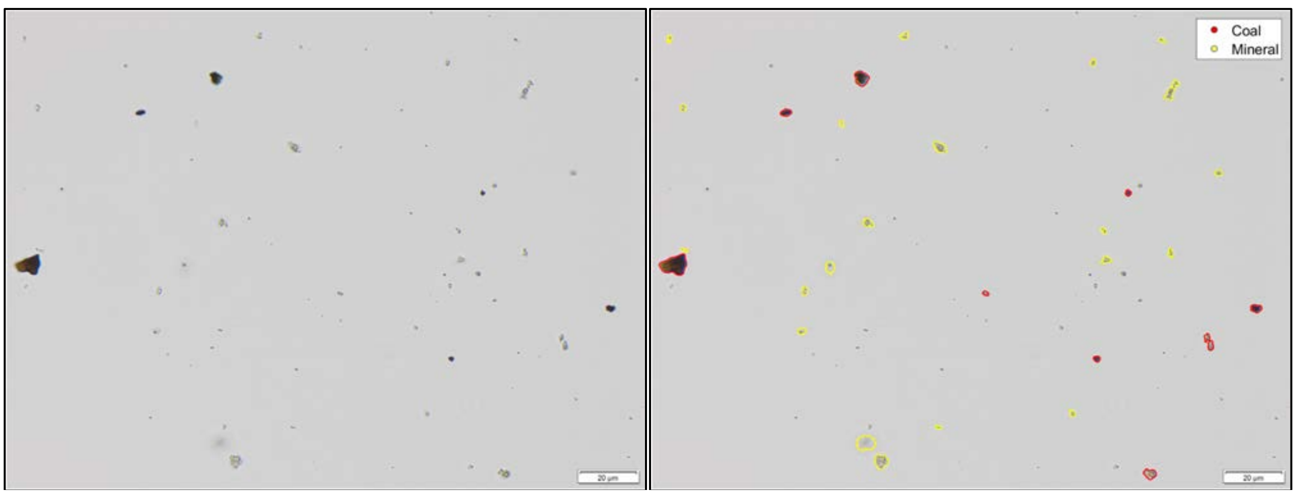

Figure 17. Coal versus mineral classification on a composite sample containing coal and kaolinite particles. Left image shows the TPP input image, and right image shows the model output with coal particles outlined in red and mineral particles outlined in yellow. Particles with no outline were not identified by the adaptive thresholding algorithm used to create the binary mask; for most such particles, the apparent reason for this is that they did not meet the 27-pixel size limit.

Classification results across all imaged frames of the composite samples are summarized in Table 9. Coal and mineral fractions were computed by summing the areas of all particles in each class and dividing by the total area of all the particles identified. This area-based approach for calculating the fractions is reasonable, since all the images and data collected are in a 2-dimensional space. For a field application, a mass-based approach would be more practical. Field testing and comparing these measurements against mass-based methods in parallel might allow finding a correlation that resembles the mass fraction of dust constituents.

Table 9 also shows the results of the SEM-EDX classification on the replicate composite samples collected on PC filters; these results were collapsed from Table 4, and again represent class percentages on an area basis. Overall, the results of the optical microscopy classification approach are in very good agreement with what was predicted by the SEM (Figure 18).

Table 9. Coal versus mineral classification results on composite samples containing coal and one mineral.

	Optical microscopy		SEM-EDX	
Sample	**Coal %**	**Mineral %**	**Coal %**	**Mineral %**
Coal + Kaolinite	27	73	26	74
Coal + Rock dust	77	23	87	13
Coal + Silica	97	3	95	5

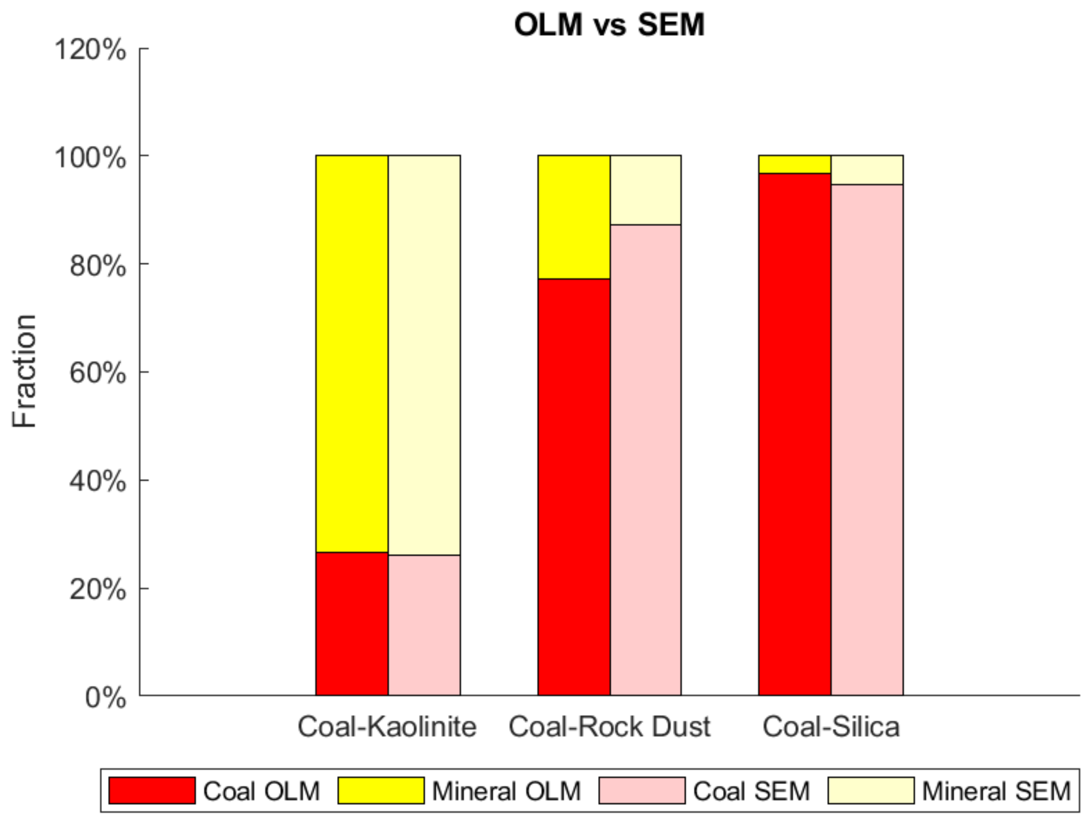

Figure 18. Coal and mineral fractions in composite samples containing coal and one mineral. Classification results are shown for the optical microscopy approach using the transmitted light AMPI model, and for the SEM for comparison.

4.2 Mineral Sub-classification (Objective 3)

The coal versus mineral classification (AMPI) model described in Section 3.2 and the silica classification (MMPI) model described in Section 3.3 were applied in series to all of the composite samples shown in Table 5. Results are tabulated in Table 10 to show the relative percentage of coal, silica and other minerals predicted, along with the results per the SEM for comparison. Figure 19 shows the results graphically. Example images with the classification results are shown in Figure 20, Figure 21 and Figure 22.

Table 10. Coal and silica classification results on composite samples containing coal and one mineral, and all three minerals. (MMPI model threshold = 0.85E+06)

	Optical microscopy			SEM-EDX		
Sample	**Coal %**	**Mineral %**	**Silica %**	**Coal %**	**Mineral %**	**Silica %**
Coal + Kaolinite	26.54	60.98	12.48	26.21	73.79	0.00
Coal + Rock dust	77.15	15.71	7.14	87.37	12.63	0.00
Coal + Silica	96.76	2.36	0.88	95.07	0.07	4.86
K+RD+S (CS1)	0.16	95.49	4.35	0.07	76.07	23.85
K+RD+S (CS2)	0.11	97.64	2.25	0.00	80.97	19.03
K+RD+S (CS3)	0.16	97.34	2.50	0.00	84.52	15.48
K+RD+S+C (CS4)	8.55	82.84	8.60	22.85	76.27	0.87
K+RD+S+C (CS5)	6.02	85.02	8.96	16.74	70.41	12.85

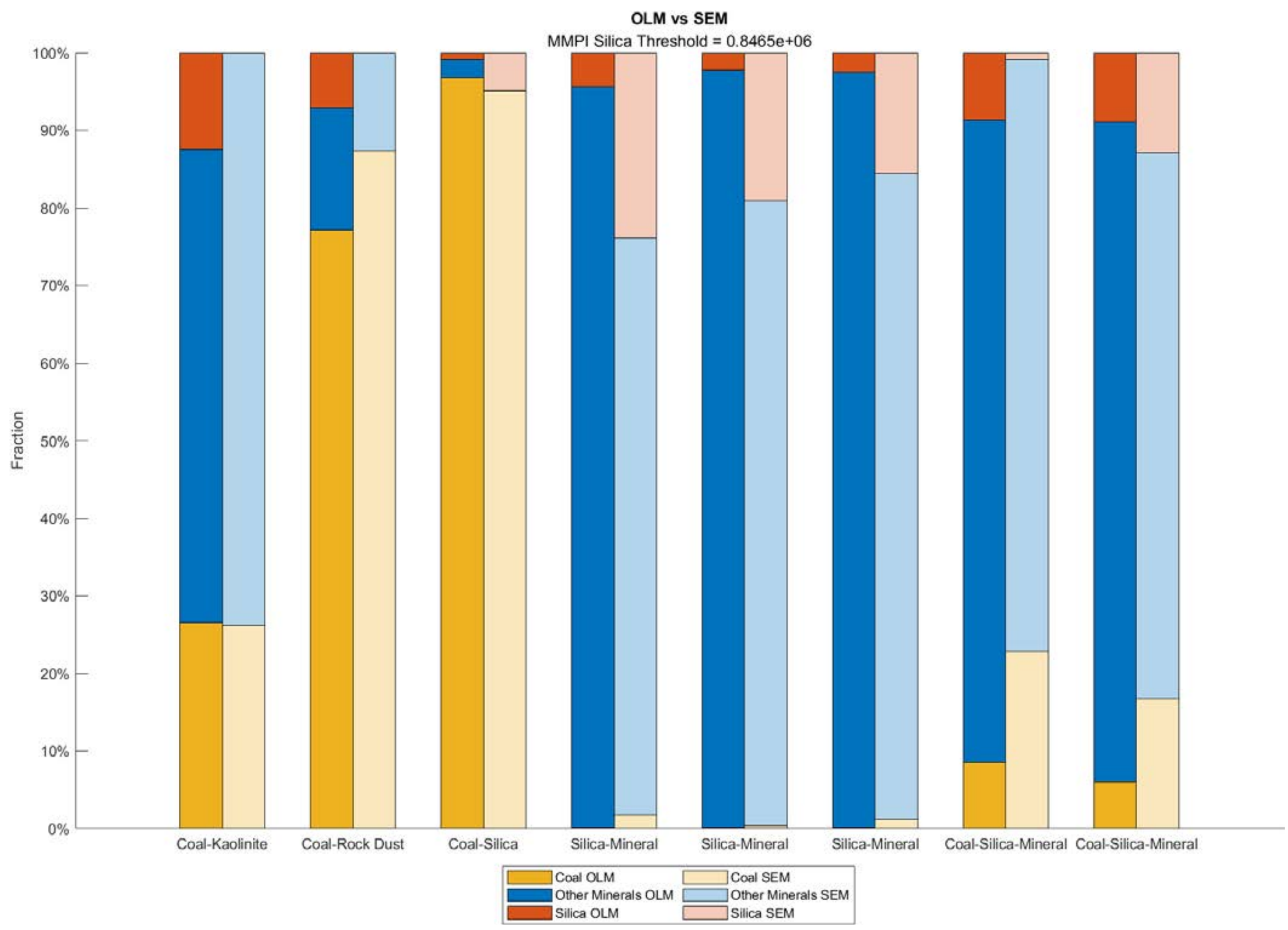

Figure 19. Coal, silica and other minerals fractions in (from left): three composite samples containing coal and one mineral, three composite samples containing all three minerals, and two composite samples containing coal and all three minerals. Classification results are shown for the optical microscopy approach using the transmitted light AMPI model (coal versus minerals) and/or MMPI model (silica versus other minerals), and for the SEM for comparison. (MMPI model threshold = 0.85E+06.)

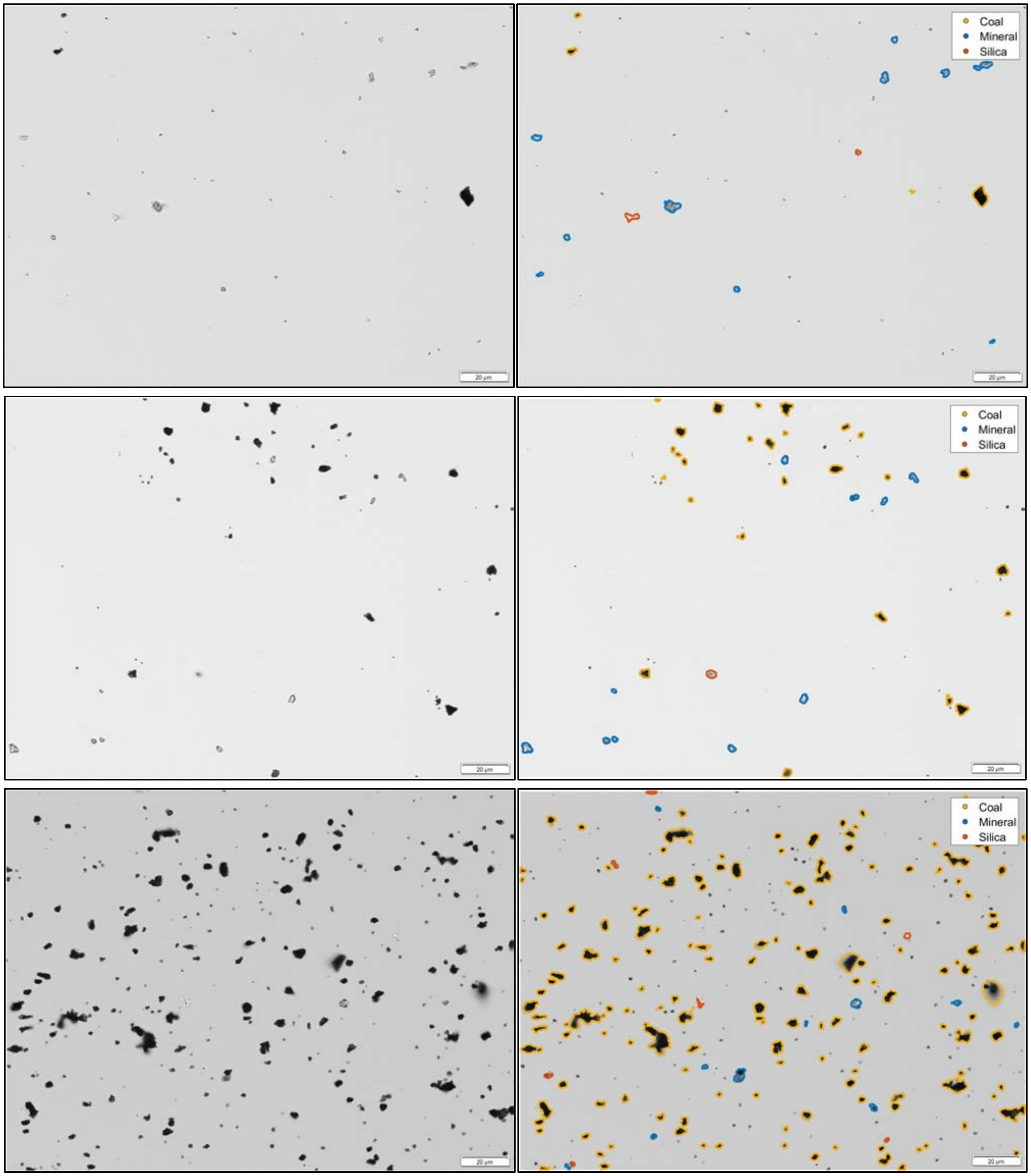

Figure 20. Coal, silica and other minerals classification on composite samples containing (top) coal and kaolinite, (middle) coal and rock dust, and (bottom) coal and silica particles. Left image in each row shows the TPP input image, and right image shows the model output with coal outlined in yellow, silica outlined in red, and other mineral particles outlined in blue. Particles with no outline were not identified by the adaptive thresholding algorithm used to create the binary mask; for most such particles, the apparent reason for this is that they did not meet the 27-pixel size limit.

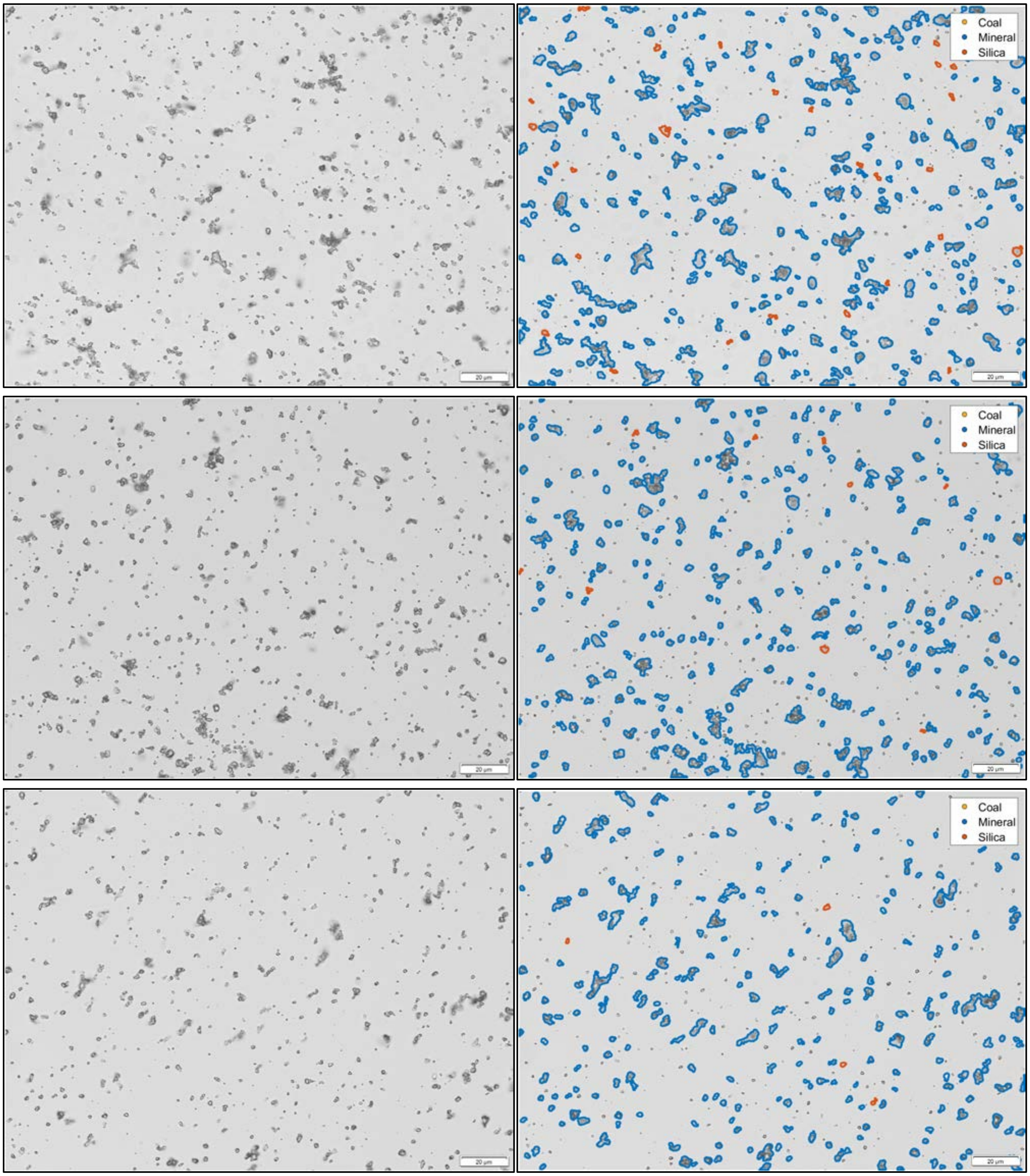

Figure 21. Coal, silica and other minerals classification on composite samples containing all three minerals. (Top) sample CS1, (middle) sample CS2, and (bottom) sample CS3. Left image in each row shows the TPP input image, and right image shows the model output with coal outlined in yellow, silica outlined in red, and other mineral particles outlined in blue. Particles with no outline were not identified by the adaptive thresholding algorithm used to create the binary mask; for most such particles, the apparent reason for this is that they did not meet the 27-pixel size limit.

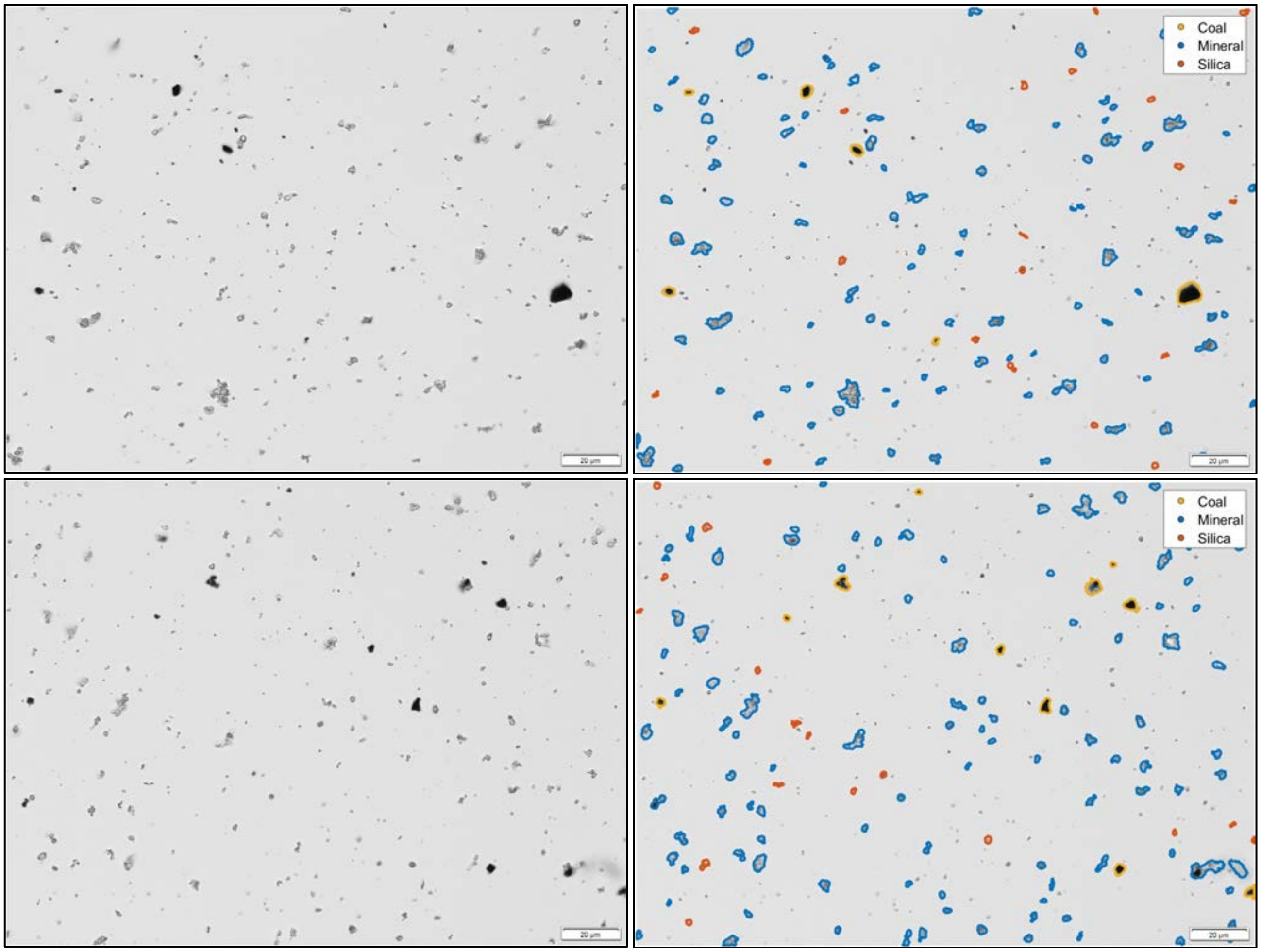

Figure 22. Coal, silica and other minerals classification on composite samples containing coal plus all three minerals. (Top) sample CS and (bottom) sample CS5. Left image in each row shows the TPP input image, and right image shows the model output with coal outlined in yellow, silica outlined in red, and other mineral particles outlined in blue. Particles with no outline were not identified by the adaptive thresholding algorithm used to create the binary mask; for most such particles, the apparent reason for this is that they did not meet the 27-pixel size limit.

The coal classification results in Figure 19 for the samples containing coal plus one mineral are identical to Figure 18, since the first step in processing the images in Figure 19 was to apply the coal versus mineral AMPI model used before. Moreover, the finding of virtually no coal in the samples containing all three minerals (but not coal) confirms that the AMPI model is working well in terms of avoiding false classification of mineral particles as coal. The fact that the SEM finds some coal (classified as mixed carbonaceous, MC) in these samples may help explain at least some of the 10-12% apparent underestimation in the coal prediction by the optical microscopy approach. Indeed, the mixed carbonaceous (MC) class in our SEM routine can occasionally include mineral (typically alumino-silicate) particles that are influenced by the filter background, in addition to include coal particles that are influenced by nearby mineral particles. For the purposes of comparing the optical microscopy and SEM results here, we have chosen to estimate coal % using the SEM-derived C+MC, which we generally believe should be accurate. However, we know factors such as filter loading and particle size can have some influence the SEM results. Further, it is also possible that in the composite samples containing coal+all minerals the abundance of mineral particles influences the coal in the optical microscopy method. This is discussed further below.

With regard to silica classification, the MMPI model performance was mixed. For the coal+silica sample and one of the coal+all minerals samples (CS5), the model predicts silica within 5% of the SEM result. For the other samples, the model is off by more. Table 7 indicates that about 15-20% of other minerals should be classified as silica, and about 23% of the silica should be classified as other minerals. Even with these tolerances, the model appears to substantially underpredict silica for the samples containing all-minerals (no coal), but it overpredicts silica for the coal+kaolinite, coal+rock dust, and one of the coal+all minerals samples. We believe this is primarily an issue of particle loading density, as explained below.

From Figure 23 (top left), it is clear that the MMPI values were significantly higher overall for the particles in the all-minerals (no coal) samples compared to the particles in the single-material (silica, kaolinite or rock dust) samples that used to train the model. Specifically, the figure shows that the peak of the histogram for all particles in these composite samples, which were about 20% silica on average, is around 2.3 E+06. In the single-material samples, the silica particles peaked at about 0.5+E06 and that of the other minerals was about 1.1+E06. Assuming a similar ratio holds in the composite samples, the 0.85+E06 threshold used by the model is too low to catch most of the silica particles. On the other hand, the histograms in Figure 23 for the mineral particles in the composite samples containing only coal plus either kaolinite (middle left) or rock dust (middle right) indicate that relatively many of these particles have MMPI values lower than the model threshold. Thus, the threshold is too high to properly classify these particles as "other minerals", and instead misclassifies them as silica.

We believe the most likely reason for the shifts in mineral particle MMPI values illustrated in Figure 23 is substantially different particle density in the composite sample images versus the single-material sample images used to build the silica classification model. As shown in Table 5, relative to the single-material samples, the number of particles per imaged frame was

- about 2x higher for the all-minerals composite samples, and the model underestimated silica;
- about 10x lower for the coal+kaolinite and coal+rock dust samples, and the model overestimated silica;
- relatively similar or slightly less for coal+silica and coal+all minerals samples, and the model came closest to matching the SEM results .

With increasing particle density in an image, particularly mineral particles, it appears they may be interfering with one another—with the effect of increasing MMPI values. In fact, this would also explain why the optical microscopy approach somewhat overpredicts coal particles relative to the SEM particles in the coal+all minerals samples. If a coal particle is in close proximity to mineral particles, it might be illuminate just enough to be classified as mineral (most likely silica given its lower position on the MMPI scale). All that said, we believe these effects can be successfully addressed by either using an adaptive model that accounts for particle density in an image, or more likely by controlling particle density during sampling and analysis.

For the purpose of better understanding the effect of the MMPI silica model threshold on classification results, the images from same six composite samples shown in Figure 19 were reanalyzed using an increased threshold of 1.85+E06. Results are presented in Figure 24 and Table 11. As expected from the histograms shown in Figure 23, the results on the three-mineral composite samples and the coal+silica sample agree well with the SEM data, but the higher threshold now exaggerates the overprediction of silica in the samples containing coal plus either kaolinite or rock dust.

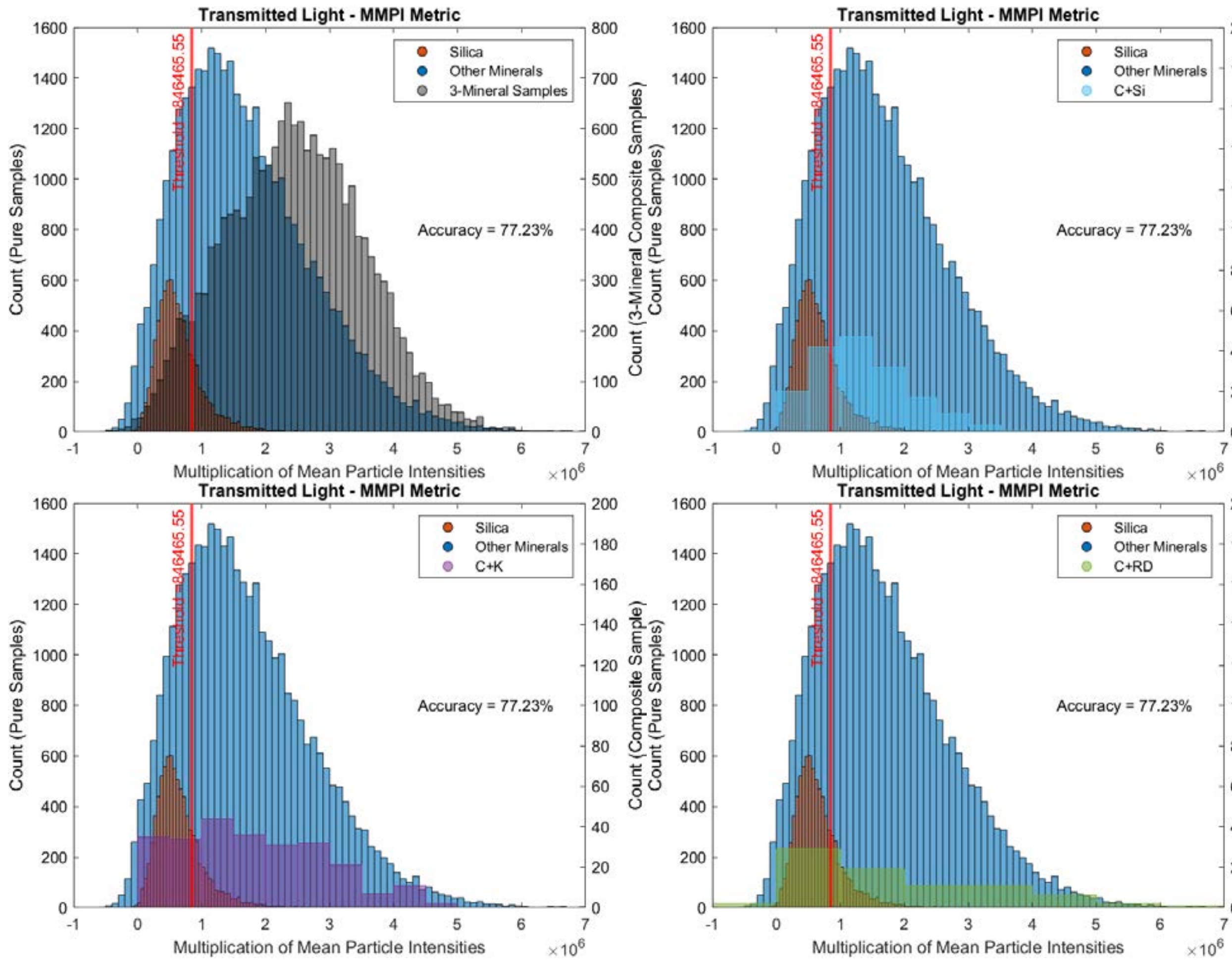

Figure 24. Distribution of MMPI values for particles in the composite samples, overlayed on the distributions of for silica and other minerals (kaolinite and rock dust) particles in the MMPI model training dataset (already shown in Figure 14). (Top left) Grey histogram shows all particles in the three-mineral composite samples; (top right) light blue shows silica particles in the coal+silica sample; (middle left) purple shows kaolinite particles in the coal+kaolinite sample; (middle right) green shows all rock dust particles in the coal+rock dust sample.

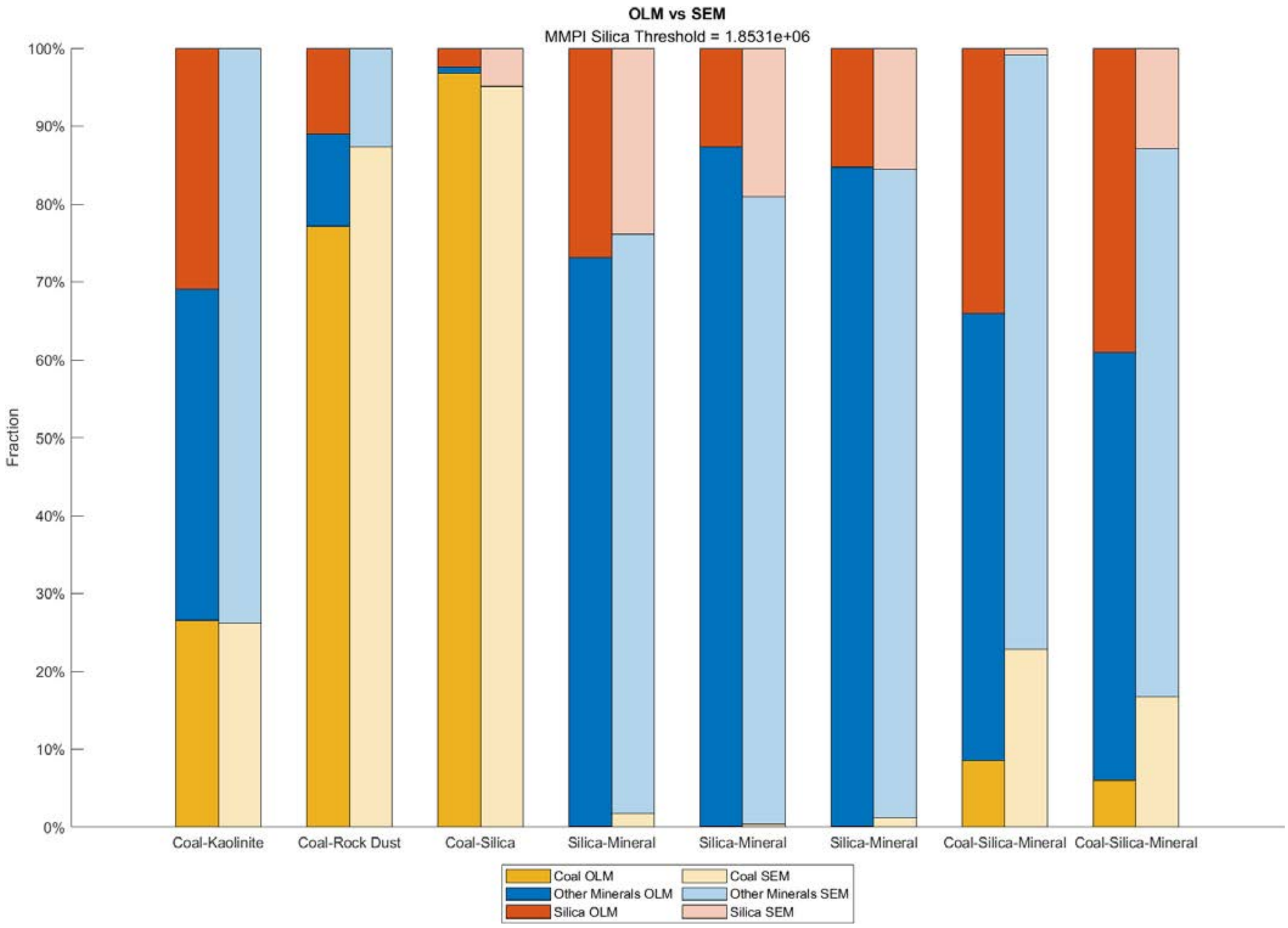

Figure 24. Coal, silica and other minerals fractions in composite samples containing coal and one mineral (left three sets of bars) and in composite samples containing all three minerals (right three sets of bars). Classification results are shown for the optical microscopy approach using the transmitted light AMPI model (coal versus minerals) and/or MMPI model (silica versus other minerals), and for the SEM for comparison. (MMPI model threshold = 0.85E+06.)

Table 11. Coal and silica classification results on composite samples containing coal and one mineral, and all three minerals. (MMPI model threshold = 1.85E+06)

	Optical microscopy			SEM-EDX		
Sample	**Coal %**	**Mineral %**	**Silica %**	**Coal %**	**Mineral %**	**Silica %**
Coal + Kaolinite	26.54	42.51	30.95	26.21	73.79	0.00
Coal + Rock dust	77.15	11.87	10.98	87.37	12.63	0.00
Coal + Silica	96.76	0.80	2.44	95.07	0.07	4.86
K+RD+S (CS1)	0.16	73.01	26.83	0.07	76.07	23.85
K+RD+S (CS2)	0.11	87.30	12.59	0.00	80.97	19.03
K+RD+S (CS3)	0.16	84.59	15.25	0.00	84.52	15.48
K+RD+S+C (CS4)	8.55	57.36	34.08	22.85	76.27	0.87
K+RD+S+C (CS5)	6.02	54.95	39.04	16.74	70.41	12.85

5.0 Publication Record and Dissemination Efforts

To date, two conference presentations have been given related to this project and the underlying concept of using optical microscopy as tool for coal mine dust monitoring:

- Santa N., Sarver E., Keles C., & Saylor J. R. (2019, May 21) Optical Microscopy: A tool for Semi-Continuous Coal Mine Dust Monitoring. In Longwall-USA 2019 Conference. Pittsburgh, PA. (*1st Place: Student Poster Award*)
  Santa, N., Sarver, E., Keles, C., & Saylor, J. (2020, Feb 25). APPLICATION OF OPTICAL MICROSCOPY FOR SEMI-CONTINUOUS COAL MINE DUST MONITORING. In 2020 SME Annual Meeting and Expo. Phoenix, AZ

Further, the work summarized in this report serves as the basis for an MS thesis:

Santa, N. (expected 2021) Demonstration of Optical Light Microscopy to Classify Respirable Dust Particles Representative of Coal Mine Environments, MS in Mining Engineering, Blacksburg, VA, USA.

We also intend to submit two full-length journal papers:

Santa, N., Sarver, E., Keles, C. & Saylor, J.R. (target submission April 2021). Demonstration of optical microscopy with polarizing light to estimate coal and mineral fractions of respirable mine dust. Aerosol and Air Quality Research.
Santa, N., Sarver, E., Keles, C. & Saylor, J.R. (target submission May 2021). Classification of major minerals in respirable coal mine dust using polarized light microscopy. Atmosphere.

6.0 Conclusions and Impact Assessment

The work presented here underpins a novel dust monitoring concept that uses a portable instrument to sample dust on a semi-continuous basis, and an on-board light microscope and image processor to classify the dust into key component fractions. To that end, this project aimed to demonstrate, for the first time, that optical light microscopy can be used to classify the major types of particles expected in respirable coal mine dust. Specifically, we sought to use established methods exploiting mineral birefringence to distinguish coal from mineral dust, and to further subclassify mineral dust into components of critical interest.

Using lab-generated dust particles from four representative source materials (i.e., high purity coal, silica, kaolinite and rock dust), we proved that coal can indeed be distinguished from the mineral particles using a relatively simple comparison between image pairs collected in plane and cross polarized light on a standard glass substrate. In plane polarized light, both coal and mineral particles are visible and can be separated from the glass background using common operations to create a binary mask image. Then, mean particle intensities in the plane polarized image can be compared with those in the cross polarized image, where the mineral particles exhibit characteristic illumination due to their birefringence. For such an approach to coal versus mineral classification, we found that use of greyscale intensities in either transmitted or reflected light should be possible, but transmitted light yielded slightly better accuracy under the conditions tested here. After training a transmitted light coal classification model using known particles (i.e., from a single source material), overall accuracy on the test dataset was about 98%. Using composite dust samples containing coal and minerals, results from the model were in very good agreement with results derived from SEM-EDX.

We additionally showed that silica classification should be possible, by exploiting differences between its birefringence and that of other primary minerals. Here, we found that respirable crystalline silica exhibited somewhat less illumination under cross polarized light than did respirable kaolinite or rock dust particles. Again using a comparison between mean particle intensities in transmitted plane and cross polarized light image pairs, we developed a silica classification model that yielded an overall accuracy of about 81% on known particles. Results on composite samples, containing coal plus one mineral, all three minerals, or coal plus all three minerals, showed mixed performance against the SEM-EDX derived data. However, this outcome appears to be mostly related to variability in particle density within the images used for model development and those captured on the composite dust samples. We believe this issue could be addressed relatively easily, either using an adaptive model that accounts for particle density in an image or by controlling particle density during sample collection.

While we were not able to demonstrate further subclassification of the other minerals investigated here (i.e., between kaolinite and rock dust), this remains a real possibility—and the work conducted on this project serves as a strong foundation.

That said, capabilities to classify coal and silica are really the top priorities for the dust monitoring concept we envision. In general, the mine face is the dustiest area of an underground coal mine and thus represents the primary target for monitoring. Given that dust in this area is predominantly influenced by the coal and rock strata being cut at the face, and not rock dusting products being applied elsewhere, the ability to track the relative abundance of coal versus mineral content in the dust can provide valuable insight to changing conditions and hazards. And silica classification, specifically, would obviously enhance hazard assessment—and deliver a highly sought advancement in near-real time dust monitoring.

Beyond routine monitoring to track key changes in dust conditions, the envisioned portable monitor could also support a range of engineering and research studies to evaluate the effects of ventilation, dust controls, equipment operating conditions and local geology on dust particles size and composition.

7.0 Recommendations for Future Work

Based on the findings from this proof-of-concept project, the following directions are recommended for future work:

- **Evaluation and correction of particle density effects on silica classification.** Follow-up work is needed to quantify the effect of particle density on the optimal threshold for silica classification using the sort of model developed here. This could be done via collection of new samples containing a range of silica content within a composite matrix, and imaging over a range of particle densities. Results could be used to incorporate a density correction into the silica classification model.
- **Demonstration of coal versus mineral classification on real mine dust particles.** The materials used here to generate respirable dust particles are representative of the major dust sources in underground coal mines, and the coal and rock dust product were in fact obtained from industry partners. However, demonstration of the coal classification method on real mine dust particles is clearly needed to further prove this capability and advance the envisioned monitoring concept.
- **Construction and testing of a prototype monitor.** Existing hardware (i.e., sampling pumps, cameras and chips) should be used to build a prototype of the envisioned optical microscope dust monitor and to perform testing in the laboratory and field.

We also note that follow-up studies could be undertaken to support further sub-classification of major mineral components—although we believe this is really secondary to the coal and silica classification capabilities demonstrated here.

8.0 References

Antao, V.C. dos S., Petsonk, E.L., Sokolow, L.Z., Wolfe, A.L., Pinheiro, G.A., Hale, J.M., Attfield, M.D. (2005). Rapidly progressive coal workers' pneumoconiosis in the United States: geographic clustering and other factors. *Occup. Environ. Med.*, 62(10), 670-674.

Ashley, E. L., Cauda, E., Chubb, L. G., Tuchman, D. P. & Rubinstein, E. N. (2020) Performance Comparison of Four Portable FTIR Instruments for Direct-on-Filter Measurement of Respirable Crystalline Silica. *Annals of Work Exposures and Health,* 64**,** 536-546.

Attfield, M., Seixas, N. (1995). Prevalence of pneumoconiosis and its relationship to dust exposure in a cohort of U.S. Bituminous coal miners and ex-miners. *Am. J. Ind. Med.*, 27(1), 137-151.

Beer, C., Kolstad, H.A., Søndergaard, K., Bendstrup, E., Heederik, D., Olsen, K.E., Omland, Ø., Petsonk, E., Sigsgaard, T, Sherson, D, Schlünssen, V. (2017). A systematic review of occupational exposure to coal dust and the risk of interstitial lung diseases. *Eur. Clin. Respir. J.*, 4(1), 1264711.

Blackley, D.J., Halldin, C.N., Laney, A.S. (2014). Resurgence of a debilitating and entirely preventable respiratory disease among coal miners*. A. J. Respir. Crit. Care Med.*, 190, 708-709.

Blackley D.J., Crum J.B., Halldin C.N., Storey E., Laney A.S. (2016). Resurgence of progressive massive fibrosis in coal Miners—Eastern Kentucky, 2016, *MMWR*, 65, 1385–1389.

Blackley, D.J., Reynolds, L.E., Short, C., Carson, R., Storey, E., Halldin, C.N., Laney, A.S. (2018). Progressive Massive Fibrosis in Coal Miners From 3 Clinics in Virginia, *JAMA*, 319(5), 500-501.

Cauda, E., Miller, A., Drake P. (2016). Promoting early exposure monitoring for respirable crystalline silica: Taking the laboratory to the mine site*. J. Occup. Environ. Hyg.,* 13(6): D39-D45.

Cohen, R., Petsonk, E., Rose, C., Young, B., Reiger, M., Najmuddin, A., Abraham, J., Churg, A., Green, F. (2016). Lung Pathology in U.S. Coal Workers with Rapidly Progressive Pneumoconiosis Implicates Silica and Silicates*. A. J. Respir. Crit. Care Med.*, 193(6), 673–680.

D'Ambrosio, M. V., Bakalar, M., Bennuru, S., Reber, C., Skandarajah, A., Nilsson, L., Fletcher, D. A. (2015). Point-of-care quantification of blood-borne filarial parasites with a mobile phone microscope. *Sci. Transl. Med.,* 7(286), 286re4.

Doney, B., Blackley, D., Hale, J., Halldin, C., Kurth, L., Syamlal, G., Laney, S. (2019) Respirable coal mine dust in underground mines, United States, 1982-2017, *Am. J Ind. Med.* 62(6): 478-485.

Gamble, J.F., Reger, R.B., Glenn, R.E. (2011). Rapidly Progressing Coal Workers Pneumoconiosis as a Con-founding Risk Factor in Assessing Coal Mine Dust Safe Exposure Levels. *J. Clin. Toxicol.*, S:1.

Hall, N., Blackley, D., Halldin, C., Laney, S. (2019) Continued increase in prevalence of r-type opacities among underground coal miners in the USA, *Occup. Environ. Med*. 76:479-481.

Jelic, T.M., Estalilla, O.C., Sawyer-Kaplan, P.R., Plata, M.J., Powers, J.T., Emmett, M., Kuenster, J.T. (2017). Coal mine dust desquamative chronic Interstitial pneumonia: A precursor of dust-related diffuse fibrosis and of emphysema. *Int. J. Occup. Environ. Med.*, 8, 153-165.

Johann-Essex, V., Keles, C., Rezaee, M., Scaggs-Witte M., Sarver, E. (2017a). Respirable coal mine dust characteristics in samples collected in central and northern Appalachia. *Int. J. Coal Geol.*, 182, 85-93.

Johann-Essex, V., Keles, C., Sarver, E. (2017b). A Computer-Controlled SEM-EDX Routine for Characterizing Respirable Coal Mine Dust. *Minerals*, 7(15).

Khaliullina, T., Kisin, E., Yanamala, N., Guppi, S., Harper, M., Lee, T., Shvedova, A. (2019). Comparative cytotoxicity of respirable surface-treated/untreated calcium carbonate rock dust particles in vitro. *Toxicology and Applied Pharmacology*, 362, 67-76.

Miller, A.L., Weakley, A.T., Griffiths, P.R., Cauda, E.G., & Bayman, S. (2017). Direct-on-filter α-quartz estimation in respirable coal mine dust using transmission Fourier Transform Infrared Spectrometry and partial least squares regression. *Appl. Spectrosc*., 71(5), 1014-1024.

Mischler, S.E., Cauda, E.G., Di Giuseppe, M., McWilliams, L.J., St. Croix, C., Sun, M., Franks, J, Ortiz, L.A. (2016). Differential activation of RAW 264.7 macrophages by size-segregated crystalline silica. *J. Occup. Med. Toxicol*., 11, 57.

Petsonk E.L., Rose, C., Cohen, R (2013). Coal mine dust lung disease. New lessons from an old exposure. *A. J. Respir. Crit. Care Med.,* 187(11), 1178–1185.

Pollock, D.E., Potts, J.D., Joy, G.J. (2010). Investigation into dust exposures and mining practices in mines in the southern Appalachian Region. Mining Engineering, 62(2), 44-49.

Sarver, E., Keles, C. & Rezaee, M. (2019) Beyond conventional metrics: Comprehensive characterization of respirable coal mine dust. *International Journal of Coal Geology,* 207**,** 84-95.

Suarthana, E., Laney, A., Storey, E., Hale, J., Attfield, M. (2011). Coal workers' pneumoconiosis in the United States: regional differences 40 years after implementation of the 1969 Federal Coal Mine Health and Safety Act. *Occup. and Environ. Med.,* 68, 908–913.

Switz, N.A., D'Ambrosio, M.V., Fletcher, D.A. (2014), Low-Cost Mobile Phone Microscopy with a Reversed Mobile Phone Camera Lens. *PLoS ONE*, 9(5): e95330.

Vallurupalli, S., Chawla, K., Kupfer, Y., Tessler, S. (2013). Mixed dust pneumoconiosis occurring in an unusual setting. *BMJ Case Reports*, bcr2013200976.

9.0 Appendix

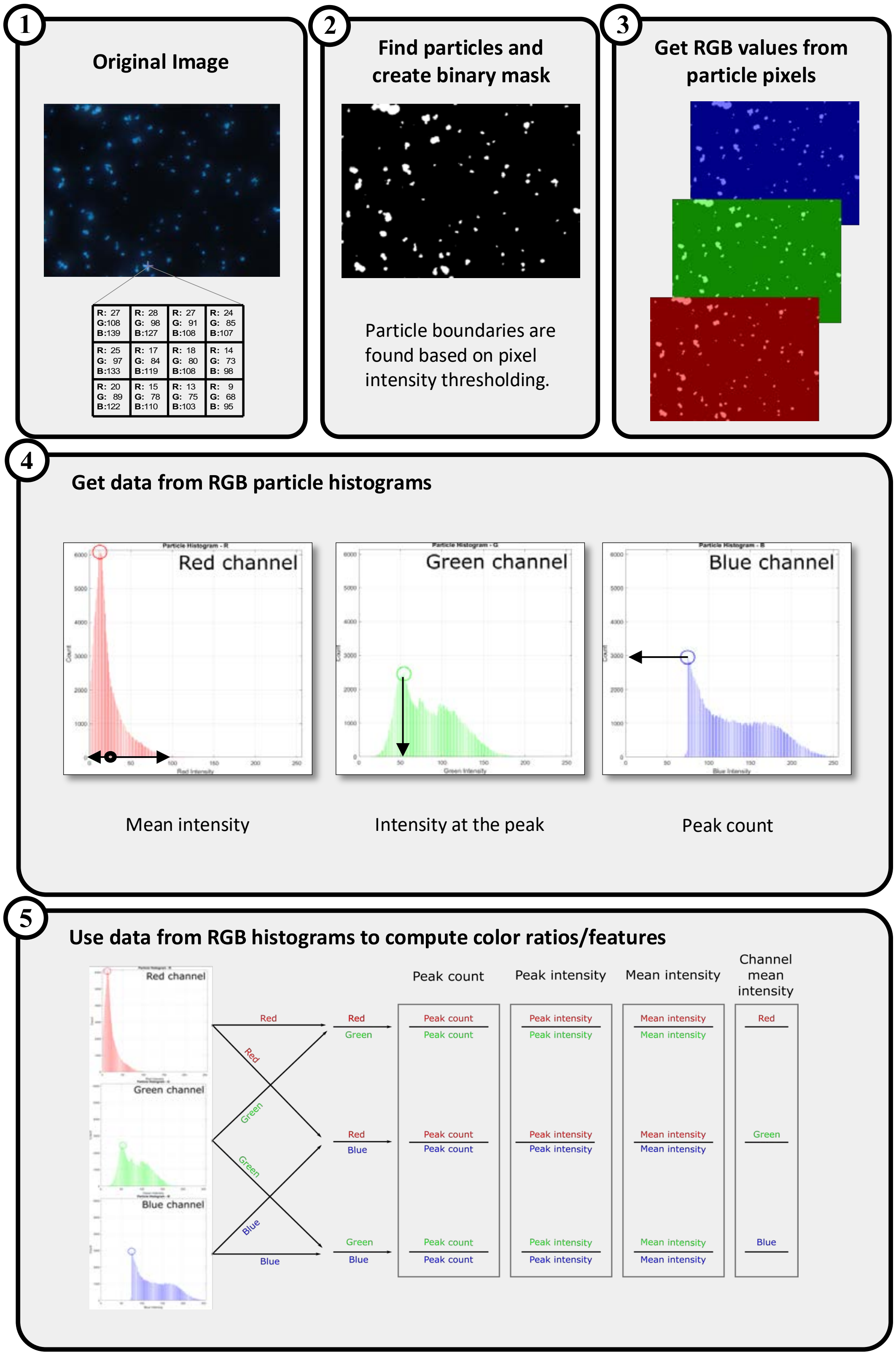

Figure A1. Schematic of the overall process to identify particles and extract particle features from a given image. This figure shows extraction of color features, but the same process can be used to extract greyscale, size/shape, and texture features.

Table A1. Particle features considered for mineral sub-classification.

	Color	Grayscale	Particle Size/Shape	Particle Texture
1	Red channel mean particle intensity (R)	Grayscale particle intensity deviation	Area	Contrast
2	Green channel mean particle intensity (G)	Grayscale aggregated mean particle intensity (AMPI)	Circularity	Correlation
3	Blue channel mean particle intensity (B)	Grayscale subtraction of mean particle intensities	Perimeter	Energy
4	R/G ratio	Grayscale multiplication of mean particle intensities (MMPI)	Max Feret Diameter	Homogeneity
5	R/B – ratio		Min Feret Diameter	
6	G/B – ratio		Aspect Ratio	
7	Red intensity at peak count (RpeakInt)		X-Diameter	
8	Green intensity at peak count (GpeakInt)		PAD	
9	Blue intensity at peak count (BpeakInt)		Perimeter/Area	
10	Max count in red channel (RpeakCount)			
11	Max count in green channel (GpeakCount)			
12	Max count in blue channel (BpeakCount)			
13	RpeakInt/ GpeakInt – ratio			
14	RpeakInt/ BpeakInt – ratio			
15	GpeakInt/ BpeakInt – ratio			
16	RpeakCount/ GpeakCount – ratio			
17	RpeakCount/ BpeakCount – ratio			
18	GpeakCount/ BpeakCount – ratio			
19	Red aggregated mean particle intensity			
20	Green aggregated mean particle intensity			
21	Blue aggregated mean particle intensity			
22	Particle intensity deviation in red channel			
23	Particle intensity deviation in green channel			
24	Particle intensity deviation in blue channel			

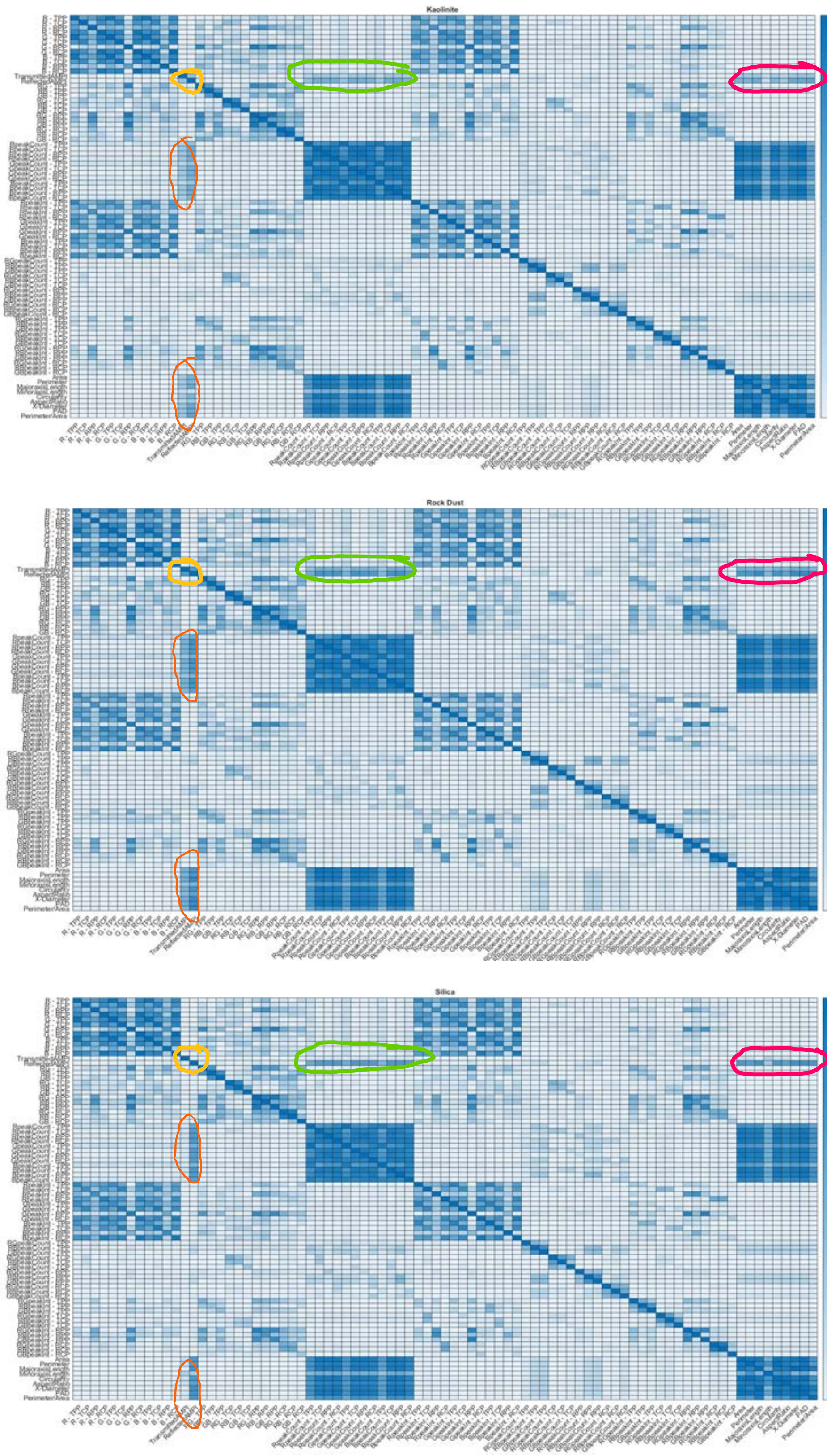

Figure A2. Correlation matrixes showing visible differences between the greyscale AMPI metrics for kaolinite (top), rock dust (middle) and silica (bottom).